JGR Oceans

RESEARCH ARTICLE
10.1029/2020JC016505

Autonomous Observation of Seasonal Carbonate Chemistry Dynamics in the Mid-Atlantic Bight

Elizabeth K. Wright-Fairbanks[1], Travis N. Miles[1], Wei-Jun Cai[2], Baoshan Chen[2], and Grace K. Saba[1]

[1]Department of Marine and Coastal Sciences, School of Environmental and Biological Sciences, State University of New Jersey at Rutgers, New Brunswick, NJ, USA, [2]School of Marine Science and Policy, University of Delaware, Newark, DE, USA

Key Points:
- A Slocum glider with an integrated deep-sea pH sensor collected high-resolution carbonate chemistry data in the Mid-Atlantic Bight
- Highest pH occurred in winter shelf and fall shelf break water, while lowest pH was seen in nearshore surface and Cold Pool bottom water
- Seasonal and spatial carbonate chemistry dynamics were influenced by stratification, freshwater input, biology, and water mass mixing

Supporting Information:
- Supporting Information S1
- Table S1
- Table S2
- Table S3

Correspondence to:
E. K. Wright-Fairbanks,
ekw31@marine.rutgers.edu

Citation:
Wright-Fairbanks, E. K., Miles, T. N., Cai, W.-J., Chen, B., & Saba, G. K. (2020). Autonomous observation of seasonal carbonate chemistry dynamics in the Mid-Atlantic Bight. *Journal of Geophysical Research: Oceans*, *125*, e2020JC016505. https://doi.org/10.1029/2020JC016505

Received 16 JUN 2020
Accepted 17 OCT 2020
Accepted article online 22 OCT 2020

Abstract Ocean acidification alters the oceanic carbonate system, increasing potential for ecological, economic, and cultural losses. Historically, productive coastal oceans lack vertically resolved high-resolution carbonate system measurements on time scales relevant to organism ecology and life history. The recent development of a deep ion-sensitive field-effect transistor (ISFET)-based pH sensor system integrated into a Slocum glider has provided a platform for achieving high-resolution carbonate system profiles. From May 2018 to November 2019, seasonal deployments of the pH glider were conducted in the central Mid-Atlantic Bight. Simultaneous measurements from the glider's pH and salinity sensors enabled the derivation of total alkalinity and calculation of other carbonate system parameters including aragonite saturation state. Carbonate system parameters were then mapped against other variables, such as temperature, dissolved oxygen, and chlorophyll, over space and time. The seasonal dynamics of carbonate chemistry presented here provide a baseline to begin identifying drivers of acidification in this vital economic zone.

Plain Language Summary Seawater chemistry affects the ability of organisms to survive in the ocean. Past monitoring of seawater chemistry has missed key times and locations that are important to natural life cycles. In order to fill in those gaps, we put a chemical sensor into a deep-sea robot that we can control from land. This robot, called a Slocum glider, glides from the top of the ocean down to 200-m depth and collects ocean chemistry data along the way. We used our Slocum glider to measure how seawater chemistry differs between seasons in the Mid-Atlantic, which will help us understand how organisms might be affected by water conditions.

1. Introduction

Ocean acidification (OA) results from the uptake of atmospheric carbon dioxide (CO_2), which alters oceanic carbonate chemistry (Doney et al., 2009; Gledhill et al., 2015; Orr et al., 2005). The ocean has absorbed approximately one third of the CO_2 emitted by human activities since the Industrial Revolution (Gruber et al., 2019). During this time, atmospheric CO_2 has risen from approximately 280 parts per million (ppm) to 410 ppm (Dlugokencky & Tans, 2020). When CO_2 is absorbed by the ocean, it reacts with seawater and results in complex chemical reactions that reduce seawater pH and calcium carbonate saturation state, Ω. Saturation states governing the formation and dissolution of the two mineral forms of calcium carbonate, calcite and aragonite, are expressed as Ω_{cal} and Ω_{arag}, respectively. A saturation state above 1 indicates carbonate supersaturation and thermodynamic favorability of carbonate calcification, while a saturation state below 1 indicates carbonate undersaturation and thermodynamic favorability of carbonate dissolution. However, carbonate saturation states approaching 1, and as high as 1.92, have been shown to cause negative impacts on calcifying organisms, despite carbonate supersaturation (Gazeau et al., 2007; Gledhill et al., 2015; Gobler & Talmage, 2013, 2014; Hettinger et al., 2012; Talmage & Gobler, 2009, 2010; Waldbusser et al., 2014), likely due to impacts on metabolism and increases in the energetic cost of mitigating stress (Melzner et al., 2019; Miller et al., 2009; Pan et al., 2015).

The rate of oceanic uptake of atmospheric CO_2 has increased in the last two decades due to increasing levels of atmospheric CO_2 (Intergovernmental Panel on Climate Change [IPCC], 2019). The global ocean is acidifying at unprecedented rates, with open ocean surface water pH decreasing by 0.017–0.027 pH units per decade

since the late 1980s (Gledhill et al., 2015; IPCC, 2019; Sutton et al., 2016; Zeebe, 2012). Global surface ocean pH is predicted to decline by up to 0.29 pH units by 2081–2100 relative to 2006–2015 under RCP8.5 (IPCC, 2019). In addition to global changes in pH, the rate of change in global Ω_{arag} since the Industrial Revolution has been 5 times greater than natural variability over the last millennium (Friedrich et al., 2012; Gattuso et al., 2015). Under RCP8.5, there will be no ocean water with Ω_{arag} greater than 3.0, and the total volume of water with Ω_{arag} less than 1.0 will increase from 76% (1990 value) to 91%, by 2100 (Gattuso et al., 2015).

In coastal oceans, carbonate chemistry is influenced by a range of drivers including productivity-respiration cycles, nutrient loading, freshwater inputs, and other coastal processes (Gledhill et al., 2015; Saba, Goldsmith, et al., 2019). Because of its multiple contributors, acidification in coastal zones can be highly variable and episodic both spatially and temporally (Baumann & Smith, 2017). The hydrodynamic and biological processes influencing coastal environments can vary on the order of minutes to days (Runcie et al., 2018; Xu et al., 2017). These extreme short-term events likely have a more immediate impact on carbonate-dependent organisms compared to gradual change due to increases in atmospheric CO_2 (Baumann & Smith, 2017; Cai et al., 2011; Waldbusser & Salisbury, 2014). However, a global increase in atmospheric CO_2 will increase the frequency of extreme acidification events, pushing organisms past critical survival thresholds more regularly (Gledhill et al., 2015). Furthermore, acidification can cooccur with other metabolic stressors, including low dissolved oxygen (DO) and warm temperatures (Cai et al., 2011, 2017; Saba, Goldsmith, et al., 2019).

The Mid-Atlantic Bight (MAB), located within the U.S. Northeast Shelf (NES), is an ecologically and economically vital coastal zone. This region is home to some of the most profitable commercial and recreational fisheries in the United States (Colvocoresses & Musick, 1984; Hare et al., 2016; NEFSC, 2020), ecosystems that protect coastal communities from inundation, storms, and erosion (NRC, 2010), and offshore wind energy development sites (Musial et al., 2013; NEFSC, 2020). The MAB is prone to acidification due to freshwater sources (primarily riverine), eutrophication and photosynthesis-respiration cycles, coastal upwelling, and other influences. Coastal inputs and biological activity alter carbonate chemistry more quickly than gas equilibrium and therefore play a major role in determining the carbonate system, specifically the partial pressure of CO_2 (pCO_2) and pH (Cai et al., 2020). Mid-Atlantic coastal waters are acutely affected by seasonal changes in temperature and inputs from shore. Because MAB oceanography is highly variable between seasons, it is necessary to monitor changes in the carbonate system seasonally (Huret et al., 2018). While there may be no net change in pH or Ω_{arag} over a full annual cycle, seasonal changes operate under a time scale that could affect biological processes in the nearshore (Gledhill et al., 2015; Waldbusser & Salisbury, 2014). Monitoring seasonal changes also provide a basis for identifying long-term changes in carbonate chemistry due to shifts in salinity, temperature, atmospheric CO_2, and coastal inputs (Gledhill et al., 2015; Goldsmith et al., 2019; Xu et al., 2020).

Acidification monitoring efforts to date are limited in temporal and spatial resolution and lacking in economically important coastal regions including the MAB (Goldsmith et al., 2019). Traditionally, monitoring in the MAB has been conducted through large field campaigns every few years. These ship-based surveys depict large spatial variability and decadal changes of surface water carbonate chemistry in the U.S. NES but lack seasonal resolution across the system (Cai et al., 2020; Z. A. Wang et al., 2013; Wanninkhof et al., 2015). In addition to cruise campaigns, there are few fixed (moored) stations monitoring carbonate system parameters on the MAB shelf. These fixed stations are capable of characterizing temporal changes in carbonate chemistry but lack spatial resolution in terms of location and depth. Additionally, many existing MAB monitoring stations measure only one of the four carbonate system parameters (pH, dissolved inorganic carbon [DIC], total alkalinity [TA], and pCO_2), two of which are necessary to fully characterize the carbonate system (Pimenta & Grear, 2018). Along with cruise campaigns and surface-fixed stations, satellite imagery can be used to estimate a suite of surface water carbon system factors, including biological productivity, pCO_2, salinity-derived carbonate parameters, and large-scale coastal inputs (Salisbury et al., 2015; H. Wang et al., 2017).

The ability to monitor carbonate chemistry in high resolution throughout the water column is critical in order to detect low pH in water masses and to derive relationships between physical, biological, and carbonate system variability. Autonomous underwater gliders, capable of collecting data in highly variable

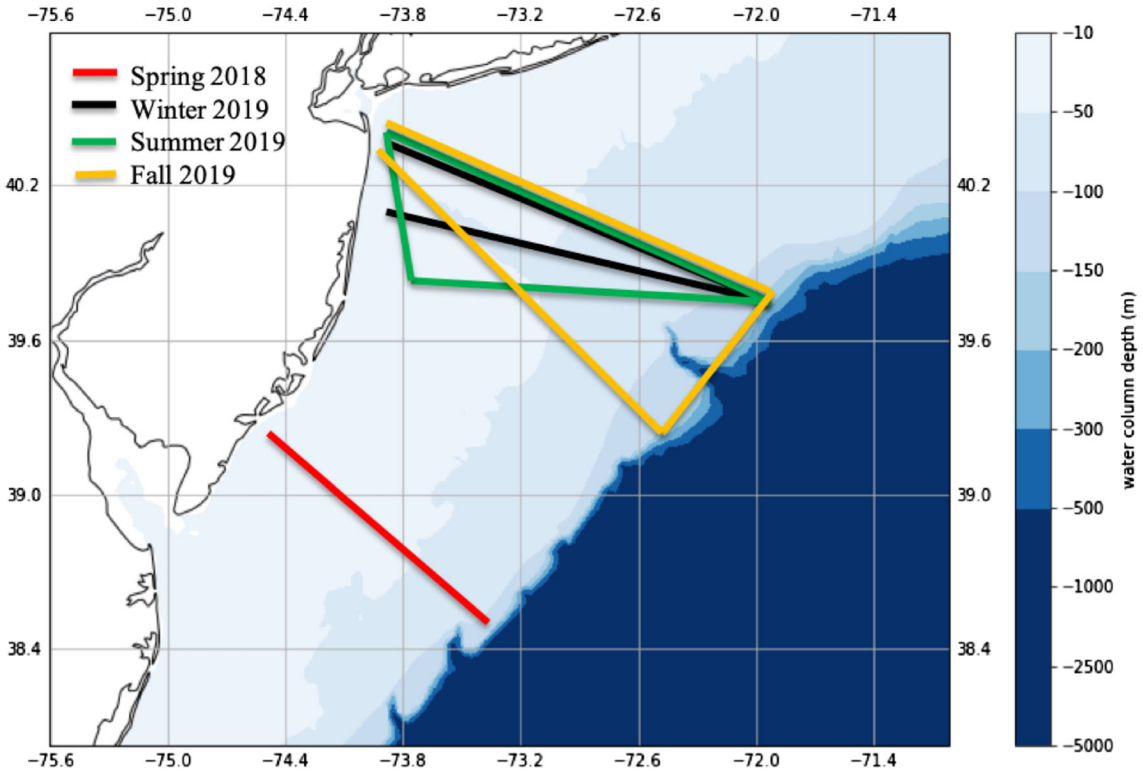

Figure 1. Seasonal glider deployments completed between May 2018 and November 2019.

currents in water depths up to 1,000 m, are a reliable platform that fulfill this role (Rudnick, 2016; Schofield et al., 2007). A deep ion-sensitive field-effect transistor (ISFET) pH sensor was recently developed and integrated into a Teledyne-Webb Slocum G2 glider (Saba, Wright-Fairbanks, et al., 2019). In addition to measuring pH, this glider has a suite of sensors that provide profiles of conductivity, temperature, DO, chlorophyll fluorescence, and spectral backscatter. This allows users to compare seawater pH to other ocean properties and conduct salinity-based estimates of TA in order to constrain the carbonate system. Here, we present data from four seasonal deployments of the pH glider in the central MAB, which have produced the first spatially and temporally high-resolution characterization of seasonal carbonate system dynamics in this region.

2. Materials and Methods

2.1. Seasonal Deployments

The pH glider was deployed on four seasonal missions in the MAB (2–22 May 2018 [spring], 1–19 February 2019 [winter], 17 July to 12 August 2019 [summer], and 15 October to 6 November 2019 [fall]; Figure 1). Before deployment, the glider pH sensor was fully conditioned following the guidelines described in Saba, Wright-Fairbanks, et al. (2019). After deployment from the small vessel R/V Rutgers, the glider was sent on a shallow mission during discrete water sample collection (see below). Once discrete sampling was completed, the glider was sent to its first offshore waypoint. The winter, summer, and fall missions followed a cross-shelf transect starting ~15 km off Sandy Hook, New Jersey, traveling 200 km eastward to the shelf break. The glider then completed various transects and triangles back to shore, covering a total of 469.6 km in winter, 503.5 km in summer, and 471.4 km in fall. The spring mission followed an established glider observation line from Atlantic City, New Jersey, 140 km eastward to the shelf break and back, for a total of 317.0 km.

Timing for sensor repairs and recalibrations prevented four sequential seasonal deployments on the Sandy Hook transect line. A mission planned for spring of 2019 on the Sandy Hook line was postponed due to technological difficulties and rough seas, and the postponed mission was terminated within hours of deployment

due to a glider pump failure. The spring deployment was rescheduled for April 2020 but was canceled due to research restrictions during the coronavirus disease 2019 (COVID-19) pandemic.

Upon each deployment and recovery of the pH glider, discrete water samples were collected following best practice guidelines for autonomous pH measurements with DuraFET sensors (Bresnahan et al., 2014; Johnson et al., 2016; Martz et al., 2015; Saba, Wright-Fairbanks, et al., 2019). Discrete samples were collected near the glider at various depths either by a hand-lowered 5-L Niskin (spring and winter; within 5 m of glider) or using an SBE55 6-bottle rosette with an SBE19 conductivity, temperature, and depth sensor (CTD) attached (summer and fall; within 100 m of glider). Samples were collected into 250-ml borosilicate glass bottles and preserved with 50 μl of saturated mercuric chloride then transported to the Cai laboratory (University of Delaware) for analysis (section 2.2.3).

2.2. Sensor QA/QC

2.2.1. Glider CTD, Oxygen, and Chlorophyll Sensors

The glider was equipped with a pumped CTD modified for integration with an ISFET pH sensor, an Aanderaa oxygen optode, and a Sea-Bird Scientific BB2FL ECO puck to measure chlorophyll fluorescence, colored dissolved organic matter (CDOM), and optical backscatter. The CTD and DO data were run through quality assurance/quality control (QA/QC) guidelines outlined in an Environmental Protection Agency (EPA) QA Project Plan for glider deployments along the coast of New Jersey (Kohut et al., 2014). Both sensors are factory calibrated annually, and data were verified predeployment and postdeployment (Saba, Wright-Fairbanks, et al., 2019). The BB2FL ECO puck is factory calibrated by WET labs every 1–2 years. Between each seasonal deployment, the integrated CTD/pH sensor was cleaned and recalibrated by the manufacturer (Sea-Bird Scientific).

2.2.2. Glider pH Sensor

Each time the glider surfaced throughout a mission, a subset of collected data was sent to shore via an Iridium satellite phone located in the tail of the glider. This allowed for preliminary inspection of all science data and software metrics to assess glider functionality. Full data sets were collected postrecovery from memory cards stored in the glider. Data were processed using Slocum Power Tools (https://github.com/kerfoot/spt/) and analyzed using MATLAB data analysis software (version R2019a).

pH data were initially inspected for sensor time lags, which were identified as skewed upcast and downcast profiles in pH reference voltage data and were often associated with areas of steep gradients in salinity or temperature. To correct for sensor lag, upcast and downcast pairs were run through potential time shifts from 0 to 60 s at 1-s intervals. The optimal time shift minimized the difference between reference voltage at a certain depth in an upcast/downcast pair (Saba, Wright-Fairbanks, et al., 2019).

After time shifts were applied, pH data were run through QA/QC measures based on the Integrated Ocean Observing System (IOOS) Manual for Real-Time Quality Control of pH Data Observations (IOOS, 2019). pH reference voltage data were flagged and removed in instances where more than 1 hr has passed between observations ($\ll$1% of observations) or in instances without a valid time stamp (~20% of observations). Next, observations of other scientific variables without both a corresponding pH reference voltage and pressure value were removed (~40% of observations). Observations outside of the latitude and longitude bounds of the MAB were flagged and removed ($\ll$1% of observations). pH values were validated in a gross range test, flagging and removing values outside the calibration bounds of the glider pH sensor (pH $<$ 6.5 and pH $>$ 9; $\ll$1% of observations). As more deployments of the pH glider provide a mean climatology for the MAB, the gross range test can be restricted to a user-specified local or seasonal pH range. Next, a spike test identified and removed single value spikes in pH reference voltage observations ($\ll$1% of observations). Lastly, data were inspected visually for unrealistic rates of change, flat-lining, and attenuated signals, which would indicate sensor failure. Tests for multivariate failure and comparisons to nearby pH sensors were not applicable to these deployments, but should be considered in future pH glider deployments.

2.2.3. Discrete Samples

Discrete sample pH was measured spectrophotometrically at 25°C using purified *meta*-Cresol Purple dye (Clayton & Byrne, 1993; Liu et al., 2011). pH accuracy was determined against Tris buffers (DelValls & Dickson, 1998; Millero, 1986). Additionally, discrete TA and DIC measurements were used to calculate pH and check the internal accuracy of spectrophotometric measurements. TA titrations were run via open cell Gran titration on an Apollo Scitech TA titrator AS_ALK2 (Cai et al., 2010; B. Chen et al., 2015;

Huang et al., 2012). DIC was quantified using a nondispersive infrared method on an Apollo Scitech DIC Analyzer AS-C3 (B. Chen et al., 2015; Huang et al., 2012). TA and DIC accuracies were determined using certified reference materials (CRMs) from Andrew Dickson's group at the Scripps Institution of Oceanography.

Discrete pH measurements were converted to in situ pH values using in situ, depth-specific temperature and salinity measured by SBE19 CTD. Discrete pH was then compared to glider ISFET measurements at the same, or closest, depth from the glider's first profile at deployment and its last profile before recovery. Groundtruthing offsets were determined as glider pH—discrete pH at each depth. Glider agreement was calculated as the average absolute offset between all depths at deployment or recovery. Uncertainty in glider agreement was calculated as one standard deviation between glider pH measurements in the surface layer during the discrete sampling period. Because there was little variation in temperature and salinity in the surface layer over a short period of time, variation in glider pH introduced by the environment was small. Glider pH science bays were sent to SeaBird Scientific for postdeployment analysis, cleaning, and recalibration between deployments.

2.3. Data Analysis

Salinity was calculated based on glider-measured conductivity, temperature, and pressure. TA and salinity exhibit a conservative relationship in U.S. East Coast waters (Cai et al., 2010; Z. A. Wang et al., 2013); thus, TA is estimated using glider-derived salinity (Saba, Wright-Fairbanks, et al., 2019). In each season, a linear regression to estimate TA from salinity was derived from a combination of discrete samples taken at glider deployment/recovery and discrete samples from transects across the U.S. NES during the East Coast Ocean Acidification (ECOA)-1 cruise in summer 2015 (supporting information Text S1). Discrete samples from glider deployments and the ECOA-1 cruise were both analyzed by the Cai group using the same method. Sampling during glider deployments and recoveries took place only in relatively low salinity nearshore waters (Figure S1). Conversely, the ECOA-1 cruise sampled across the entire shelf to the shelf break but missed lower salinity areas. Using both seasonal discrete samples and shelf-wide ECOA samples ensured that seasonal TA-salinity regressions accounted for the entire scope of salinities the glider encountered in the MAB while minimizing uncertainty due to seasonal differences in TA-salinity relationships. Full-deployment salinity-estimated TA was also compared to TA derived using the CANYON-B algorithm, which is trained on GLODAPv2 and GO-SHIP bottle samples, and calculates carbonate system parameters using measured latitude, longitude, time, depth, temperature, salinity, and oxygen (Bittig et al., 2018).

Glider pH was calculated on the total hydrogen concentration scale using glider-measured reference voltage, salinity, pressure, temperature, and sensor-specific calibration coefficients (Johnson et al., 2017; Saba, Wright-Fairbanks, et al., 2019). The remaining carbonate system parameters were calculated using CO2SYS for MATLAB (v3.0) with glider temperature, salinity, pressure, pH, and salinity-derived TA as inputs (Lewis & Wallace, 1998; Sharp et al., 2020; van Heuven et al., 2011). Other CO2SYS inputs included total pH scale (mol kg^{-1}-SW), K_1 and K_2 constants of Mehrbach et al. (1973) with refits by Dickson and Millero (1987), KSO_4 dissociation constant of Dickson (1990), KHF dissociation constant of Uppstrom (1974), and borate-to-salinity ratio of Perez and Fraga (1987). Carbonate system parameters reported here are pH, Ω_{arag}, and ratio of TA to DIC (TA:DIC). TA:DIC provides context for the CO_2 buffering capacity of seawater. Oceanic buffering capacity for CO_2 reaches a minimum at TA:DIC = 1, meaning water with TA:DIC closest to 1 is most susceptible to acidification (Cai et al., 2020; Egleston et al., 2010; Z. A. Wang et al., 2013).

Slocum gliders are propelled by purposeful changes in buoyancy, allowing the glider to dive and climb in a sawtooth pattern from surface to bottom waters. The pH glider system used here was equipped with a 200-m pump, allowing it to operate in depths as shallow as 4 m and as deep as 200 m. Coastal gliders travel approximately 20 km day^{-1} horizontally, while profiling vertically at 10–15 cm s^{-1}. Sensors sample at 0.5 Hz, providing observations at 20- to 30-cm intervals vertically. All measured and derived variables were bin-averaged into 1-m depth by 1-km-distance bins. At a sampling rate of 0.5 Hz and vertical profiling velocity of 10–15 cm s^{-1}, a 1-m depth average incorporated three to five measurements, minimizing the effect of small-scale physical and biological water column dynamics. At a horizontal speed of 20 km day^{-1}, a 1-km-distance bin averaged 1.2 hr of data, which could include between 3 and 30 individual profiles depending on water column depth.

Brunt-Vaisala frequency squared (N^2) was calculated between adjacent 1-m layers in each depth- and distance-binned profile. The mixed-layer depth (MLD) for each binned profile was determined as the depth of maximum N^2 (max(N^2)) (Carvalho et al., 2017). Each profile's mixed layer was assigned a quality index (QI), which indicates the significance of the stratification index based on relative homogeneity in and below the mixed layer (Carvalho et al., 2017; Lorbacher et al., 2006). Profiles with QI < 0.5 were considered well mixed and removed from MLD analysis.

For analysis, deployment data were split into spatial and depth-defined regions. Distinctions between surface and bottom waters were made using the mean MLD in each season, with surface waters defined as surface to MLD, and bottom waters from MLD to the bottom. During winter, there was no significant MLD (QI < 0.5). Therefore, winter surface and bottom parameters were represented by an average of the top 5 m and bottom 5 m of the water column, respectively. The nearshore region was defined as extending from shore to the 35-m isobath, where sea slope begins to increase in the central MAB, or 1–40 km offshore (Levin et al., 2018). Midshelf was defined from the 35- to 100-m isobaths or 40–160 km offshore (40–120 km offshore in the spring). The shelf break was defined as beyond the continental shelf (>160 km offshore or >120 km offshore in spring), where depth increases to >100 m.

Significances of regional and seasonal comparisons of measured and derived variables were calculated using a Kruskal-Wallis analysis with Dunn post hoc, unless otherwise noted. Significance is reported as a p value, with $p < 0.05$ demonstrating a significant difference between the values being compared. All averages are presented as mean ±1 standard deviation, and a table of averages is included in the supporting information (Table S1). Along with being depth-averaged into 1-m bins, chlorophyll and oxygen concentrations were integrated to 35-m depth to analyze mixed layer productivity. Integration to 35 m, as opposed to full-water column integration, ensured that the majority of mixed layer productivity in each season was captured while minimizing skewed integrations that could arise due to seasonal differences in profile depths. The 35-m integrated chlorophyll and oxygen are presented along with 1-m depth-averaged chlorophyll and oxygen.

To visualize the spread of data in each season, box-and-whisker plots displaying medians, 25th and 75th percentiles, minimums, and maximums were created for glider-measured and derived variables. To summarize carbonate system interactions with the development and degradation of seasonal stratification and chlorophyll maxima, physical, biological, and carbonate system properties from the first cross-shelf transect of each deployment were plotted on common color axes. Finally, full-deployment carbonate parameters were plotted as a function of distance from shore and season in order to visualize spatial differences in carbonate system seasonality.

3. Results

3.1. Sensor Performance

A full record of groundtruthing offsets is available in Tables S2 and S3. Seasonal mean glider agreement ranged from 0.005 to 0.042 pH units and within-mixed-layer variability ranged from 0.001 to 0.027 pH units. Given these observations, we believe that glider pH measurements are accurate to better than 0.05 pH units, which agrees with the manufacturer accuracy specification for this sensor (±0.05 pH units). Short-term reproducibility is likely significantly better than 0.03 because the source of error is short-term, within-mixed layer repeatability. This conclusion is supported by the manufacturer precision specification for this sensor (±0.001 pH units), which implies that spatial variability along a section can be resolved to ±0.001 pH units. Therefore, pH is reported here to the third decimal place.

pH sensor time lag varied seasonally. No shift was necessary for the winter mission, while 47- and 30-s shifts were applied to the spring mission, a 36-s shift was applied to the summer mission, and a 45-s shift was applied to the fall mission. Spring required two lag corrections because of a shift in the sensor lag between the first third and last two thirds of deployment, likely due to a shift in water column structure (Saba, Wright-Fairbanks, et al., 2019).

The magnitude of uncertainty in derived variables varied based on the accuracy of TA estimation. Average absolute differences between discrete TA and estimated TA ranged from 5.5 (winter) to 27.4 μmol kg^{-1} (summer). Average uncertainty in Ω_{arag} and TA:DIC due to TA offsets ranged from 0.005 to 0.024 and 0.0001 to 0.0003, respectively (Table S4). A full analysis of TA offsets, as well as a list of seasonal

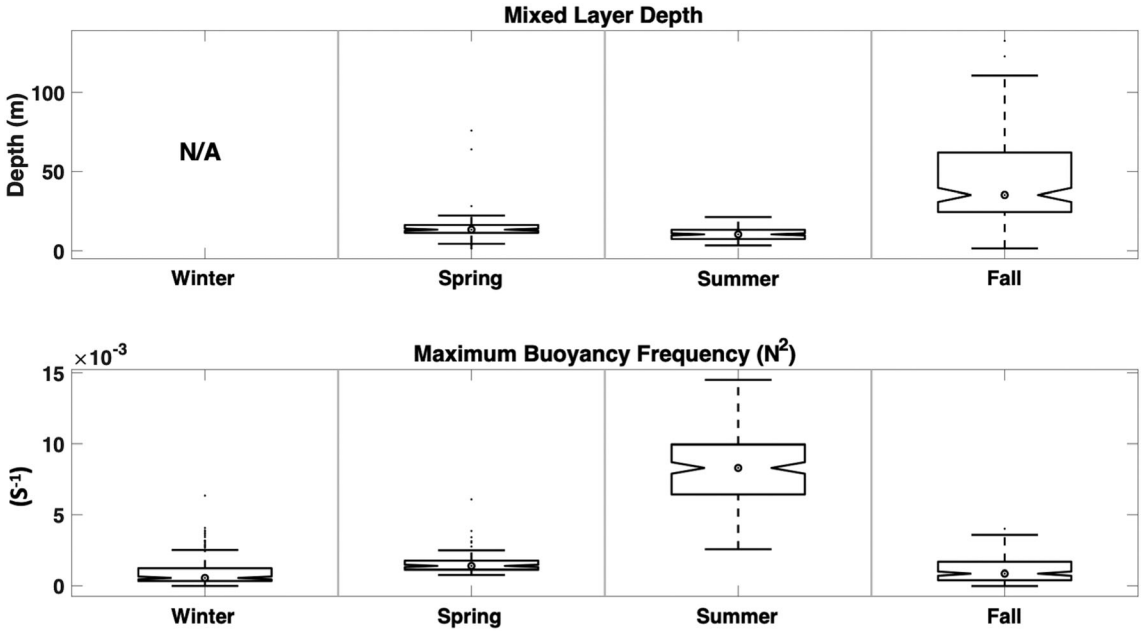

Figure 2. Comparisons of mixed layer depth (MLD) and maximum buoyancy frequency (max(N^2)) during seasonal glider deployments. Targets indicate median values, box limits indicate the 25th to 75th percentiles, and whiskers represent the full range of data. Data points beyond 1.5 times the interquartile range away from the top or bottom of the box were identified as outliers and are shown as black dots extending from the whiskers. Notches depict the 95% confidence interval around the median. If notches do not overlap, there is 95% confidence that the medians are different ($p < 0.05$). Winter had a well-mixed water column with insignificant MLD QI values; thus, no data are shown for winter MLD.

TA-salinity regressions, can be found in the supporting information (Text S1 and Tables S4 and S5). Full-deployment salinity-derived TA was similar to CANYON-B algorithm estimates of TA, differing at most by a seasonal average of 2.0 ± 4.3 μmol kg^{-1} (~0.1%).

3.2. Seasonal and Spatial Water Column Dynamics

The winter mission collected 4,933 profiles of science data over 19 days, spring collected 6,426 profiles over 20 days, summer collected 6,948 profiles over 26 days, and fall collected 5,333 profiles over 22 days. On average, about 270 profiles were generated per day. Although the four seasonal deployments were not sequential, they highlight stratification and mixing patterns typical of the MAB, revealing seasonal transitions in physical, biological, and chemical characteristics described in detail below.

3.2.1. Physical Dynamics

Seasonal changes in stratification occurred in the MAB (Figures 2 and 3). The winter water column was cold (<13°C) and well mixed, with no significant MLD (QI < 0.5) and the lowest observed max(N^2) (0.0010 ± 0.0010 s^{-1}, $n = 187$, $p < 0.001$). Surface waters were warmer in the spring compared to winter ($p < 0.001$), resulting in stronger stratification (max(N^2) = 0.0015 ± 0.0005 s^{-1}, $n = 129$, $p < 0.001$) and MLD of 14.4 ± 8.2 m ($n = 129$). Surface temperature peaked in the summer (23.64 ± 1.13°C, $n = 188$, $p < 0.001$), while bottom waters remained cold, resulting in continued shoaling of MLD to 10.4 ± 3.7 m ($n = 188$) and the greatest max(N^2) observed seasonally (0.0082 ± 0.0025 s^{-1}, $n = 188$, $p < 0.001$). Strong stratification in the spring and summer trapped a cold (<12°C) water mass below the mixed layer, which was consistent with the well-known summer Cold Pool (Z. Chen et al., 2018; Houghton et al., 1982). Surface waters cooled in the fall, causing a lower max(N^2) (0.0011 ± 0.0009, $n = 358$), and a deep MLD (44.7 ± 27.7 m, $n = 180$).

Surface and bottom water salinity were significantly lower in the nearshore than at the shelf break in every season ($p < 0.001$; Figures 3 and 4). With the exception of spring (full water column) and summer bottom water, surface and bottom temperature also increased from nearshore to the shelf break in each season ($p < 0.004$; Figures 3 and 4). The lowest salinities were recorded in nearshore summer surface waters ($p < 0.001$), averaging 30.06 ± 0.37 PSU ($n = 28$). In the summer, midshelf surface waters were also significantly fresher than the other seasons ($p < 0.001$), due to heavy rainfall during the mission. The highest

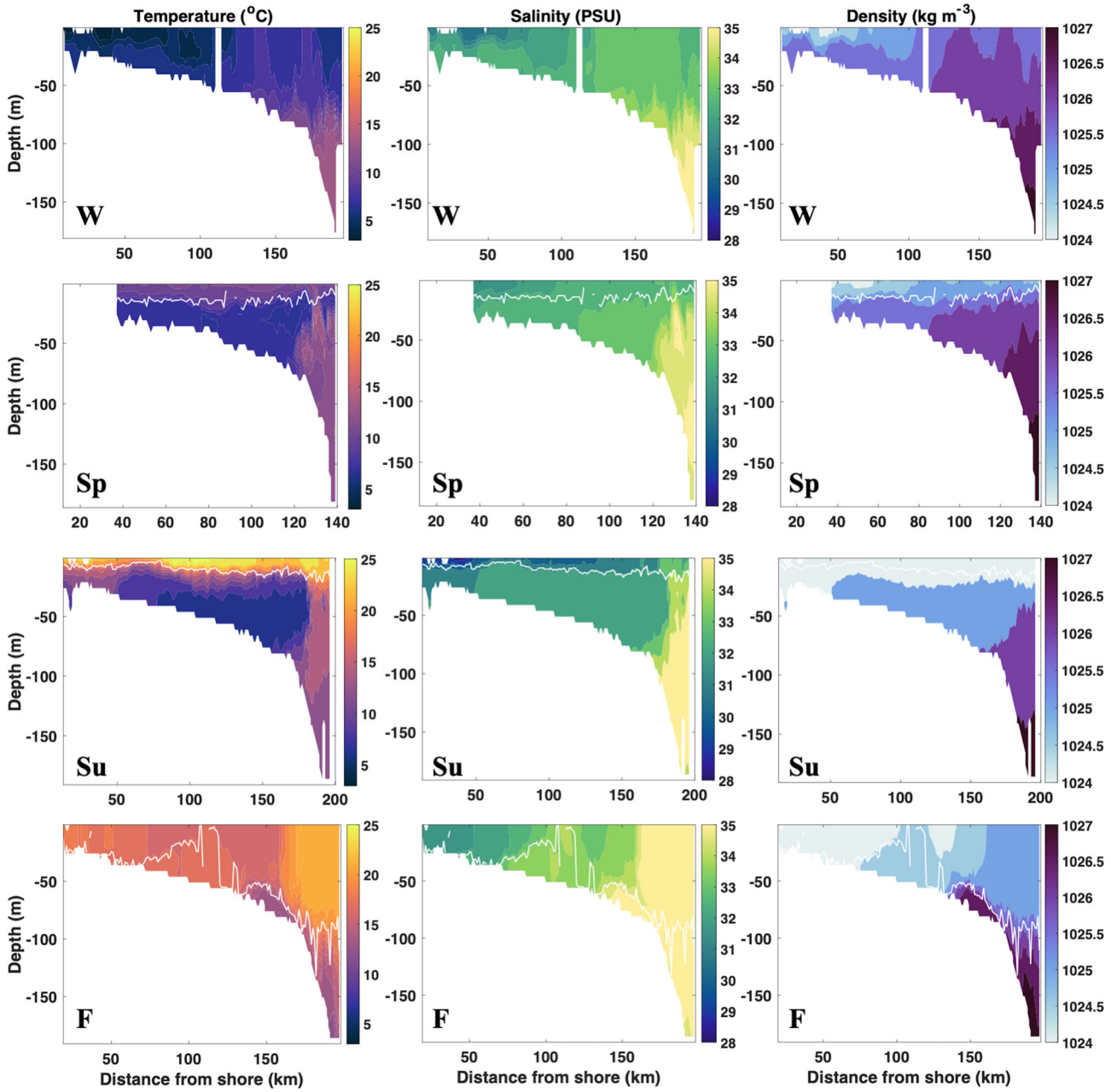

Figure 3. Contour plots of temperature, salinity, and density from four seasonal glider deployments in the MAB (W = winter, Sp = spring, Su = summer, and F = fall). Data shown are from the first cross-shelf transect of each deployment. Mixed layer depth (MLD) for each binned profile is plotted in white. Winter had no significant mixed layer. The nearshore region was defined as 1–40 km offshore, midshelf was 40–160 km offshore (40–120 km in spring), and the shelf break was >160 km offshore (>120 km offshore in spring).

salinities were recorded in fall shelf break surface and bottom waters ($p < 0.001$), averaging 35.66 ± 0.26 PSU ($n = 38$) and 35.37 ± 0.17 PSU ($n = 38$).

3.2.2. Biological Characteristics

Phytoplankton biomass varied seasonally as water column structure changed in the MAB (Figures 4 and 5). The deeply mixed fall water column and the productive spring water column had the highest 35-m integrated chlorophyll concentrations of 43.39 ± 11.23 mg m^{-2} ($n = 180$) and 42.82 ± 19.79 mg m^{-2} ($n = 129$), respectively ($p < 0.001$). Fall and spring integrated chlorophyll levels were not significantly different from one another. Winter and summer had significantly lower 35-m integrated chlorophyll concentrations than the seasons preceding them ($p < 0.001$).

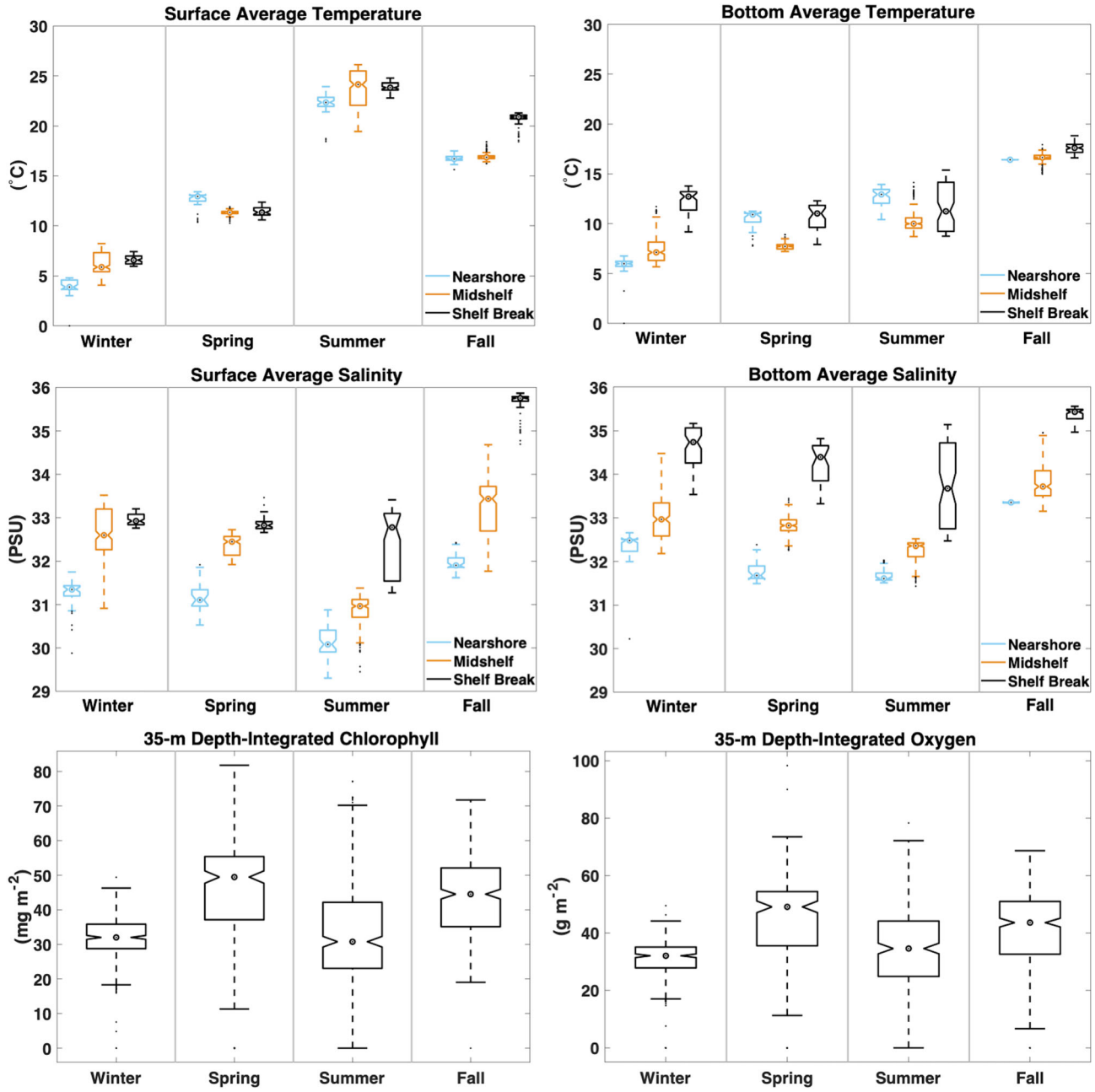

Figure 4. Comparisons of physical, biological, and chemical ocean properties during seasonal glider deployments. Targets indicate median values, box limits indicate the 25th to 75th percentiles, and whiskers represent the full range of data. Data points beyond 1.5 times the interquartile range away from the top or bottom of the box were identified as outliers, and are shown as black dots extending from the whiskers. Notches depict the 95% confidence interval around the median. If notches do not overlap, there is 95% confidence that the medians are different ($p < 0.05$).

In each binned profile, the chlorophyll maximum was identified as the 1-m depth bin with the highest 1-m depth-averaged chlorophyll concentration. Depth-averaged chlorophyll concentrations at the chlorophyll maximum were 1.55 ± 0.48 mg m^{-3} (n = 187) in winter, 3.35 ± 2.16 mg m^{-3} (n = 129) in spring, 2.52 ± 0.88 mg m^{-3} (n = 188) in summer, and 1.80 ± 0.58 (n = 180) mg m^{-3} in fall.

In each season, surface and bottom depth-averaged chlorophyll was highest in the nearshore and lowest at the shelf break ($p < 0.001$), except in fall bottom water which saw no significant spatial change (Figure 5). The highest depth-averaged chlorophyll concentrations occurred in nearshore spring bottom water (2.86 ± 0.49 mg m^{-3}, n = 13, $p < 0.001$), which captured the spring chlorophyll maximum layer. High

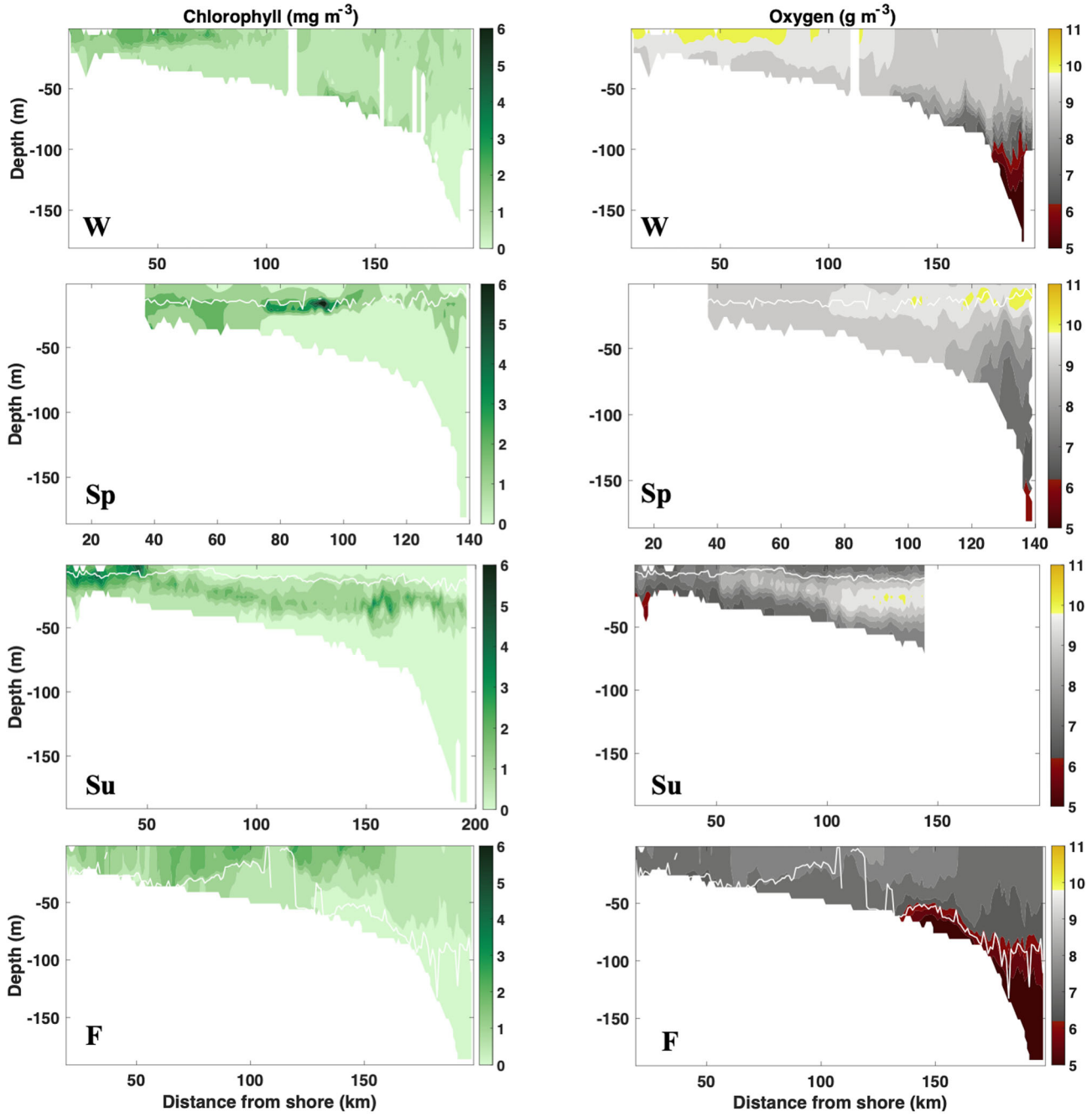

Figure 5. Contour plots of depth-averaged chlorophyll and oxygen from four seasonal glider deployments in the MAB (W = winter, Sp = spring, Su = summer, and F = fall). Data shown are from the first cross-shelf transect of each deployment. Mixed layer depth (MLD) for each binned profile is plotted in white. Winter had no significant mixed layer. The nearshore region was defined as 1–40 km offshore, midshelf was 40–160 km offshore (40–120 km in spring), and the shelf break was >160 km offshore (>120 km offshore in spring).

depth-averaged chlorophyll was also present in spring and summer nearshore surface waters, averaging 2.13 ± 0.71 mg m^{-3} (n = 13) and 2.30 ± 0.45 mg m^{-3} (n = 28), respectively.

3.2.3. Chemical Dynamics

3.2.3.1. Oxygen

The chlorophyll-rich, stratified spring and deeply mixed fall water columns exhibited the highest 35-m integrated DO concentrations of 41.55 ± 20.12 g m^{-2} (n = 129) and 41.86 ± 12.46 g m^{-2} (n = 180) ($p < 0.001$;

Figures 4 and 5). Like chlorophyll concentration, winter and summer 35 m integrated oxygen levels were significantly lower than both fall and spring ($p < 0.001$).

In spring, summer, and fall, high depth-averaged DO was observed at the chlorophyll maximum depth (Figure 5). Shelf break bottom waters exhibited the lowest depth-averaged DO concentrations in winter, spring, and fall ($p < 0.001$), averaging 6.20 ± 0.88 g m^{-3} ($n = 35$), 8.20 ± 0.49 g m^{-3} ($n = 20$), and 6.32 ± 0.36 g m^{-3} ($n = 39$), respectively. The DO optode malfunctioned shortly after summer deployment, so summer shelf break measurements are not available.

3.2.3.2. Carbonate System

Figures 6 and 7 display seasonal and spatial differences in the carbonate system. Full water column pH ranged from 7.701 to 8.166 throughout all seasons, while Ω_{arag} ranged from 0.83 to 3.72, and TA:DIC ranged from 1.019 to 1.180. Deployment-averaged pH was highest in winter and lowest in summer (Table S6). Deployment-averaged Ω_{arag} and TA:DIC were highest in fall and lowest in summer (Table S6). Areas that differed from the means were localized in space and time. For example, areas of high pH were associated with the chlorophyll maximum in spring and summer, and areas of high pH, Ω_{arag}, and TA:DIC were found at the shelf break in all seasons (Figure 6). Conversely, areas of low pH, Ω_{arag}, and TA:DIC were associated with the nearshore region in spring, summer, and fall, and with shelf bottom waters in the summer (Figure 6).

In summer and fall, surface and bottom pH, Ω_{arag}, and TA:DIC were lowest in the nearshore and significantly higher at the shelf break ($p < 0.001$; Figure 7). The highest spring pH, Ω_{arag}, and TA:DIC values were also present at the shelf break ($p < 0.005$, Figure 7). Winter followed a different spatial pattern, with surface and bottom pH highest in the nearshore and significantly lower at the shelf break ($p < 0.001$). Winter surface Ω_{arag} and TA:DIC were highest in the midshelf region ($p < 0.05$), while bottom Ω_{arag} and TA:DIC increased from nearshore to shelf break ($p < 0.002$).

In the nearshore, surface and bottom pH were highest in winter, averaging 8.124 ± 0.007 ($n = 31$) and 8.080 ± 0.014 (n = 31) respectively ($p < 0.005$; Figures 6 and 7). The lowest nearshore pH occurred in summer bottom waters ($p < 0.001$), averaging 7.827 ± 0.029 ($n = 28$). Bottom waters also reached a minimum in Ω_{arag} and TA:DIC in summer ($p < 0.03$), averaging 1.29 ± 0.11 and 1.048 ± 0.007 respectively ($n = 28$). Contrary to seasonal patterns in pH, nearshore surface water saw the highest Ω_{arag} and TA:DIC in the summer/fall and lowest in the winter/spring ($p < 0.001$).

In the midshelf, the highest seasonal pH occurred in well mixed, cold winter surface water ($p < 0.002$; Figures 3, 6, and 7). Average winter midshelf surface pH was 8.107 ± 0.013 ($n = 121$). Conversely, winter midshelf surface waters had low Ω_{arag} and TA:DIC, averaging 1.84 ± 0.09 and 1.082 ± 0.004, respectively ($n = 121$). The lowest midshelf pH occurred in summer surface and bottom water, averaging 7.934 ± 0.016 in the surface and 7.922 ± 0.053 in the bottom ($p < 0.001$, $n = 120$). Low pH summer bottom water was associated with the Cold Pool bottom water mass and also exhibited the lowest Ω_{arag} and TA:DIC in the midshelf (1.47 ± 0.15 and 1.059 ± 0.009, respectively; $p < 0.001$; $n = 120$). While summer midshelf bottom water had the lowest seasonal Ω_{arag} and TA:DIC, summer midshelf surface water had the highest values in the region, averaging 2.30 ± 0.18 and 1.101 ± 0.008 respectively ($p < 0.001$, $n = 120$), though these values were not significantly different than fall.

At the shelf break, a warm, salty water mass persisted throughout all four seasons (Figure 3). The highest shelf break Ω_{arag} and TA:DIC occurred in fall ($p < 0.001$), when this water mass mixed into the surface layer (Figure 6). There, Ω_{arag} averaged 3.13 ± 0.12 ($n = 39$) and TA:DIC averaged 1.138 ± 0.006 ($n = 39$). The lowest shelf break Ω_{arag} and TA:DIC occurred in winter surface waters ($p < 0.05$), averaging 1.73 ± 0.06 and 1.075 ± 0.003 ($n = 35$), respectively. The lowest seasonal shelf break pH occurred in summer surface waters ($p < 0.001$), averaging 7.969 ± 0.014 ($n = 39$).

4. Discussion

High-resolution data resulting from deployments of a glider equipped with novel pH sensor technology highlight seasonal and spatial carbonate chemistry dynamics in the MAB for the first time. Results underscore the importance of seasonality, water mass mixing, biological production, and freshwater inputs in controlling the carbonate system in the MAB.

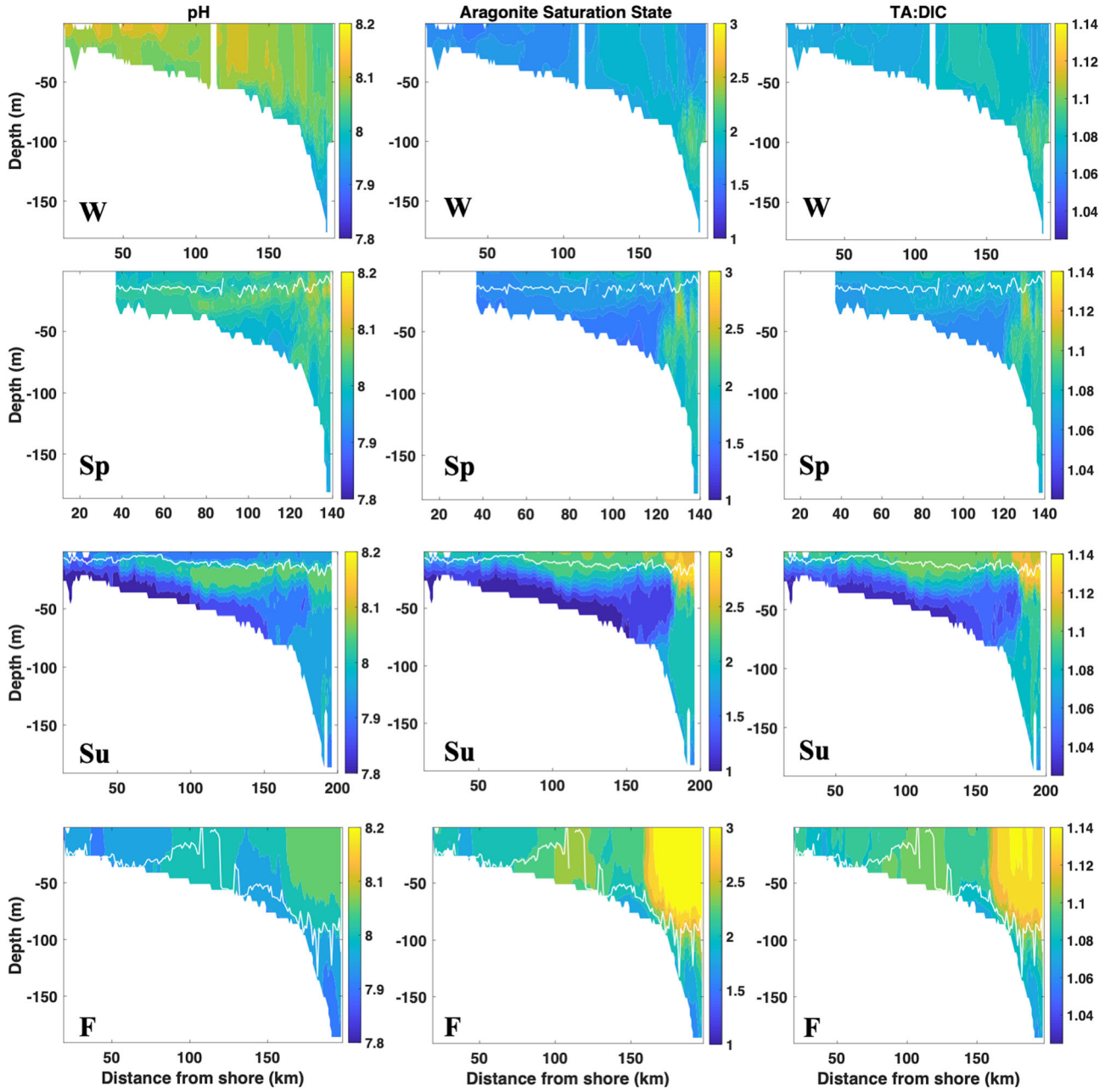

Figure 6. Contour plots of in situ pH, Ω_{arag}, and TA:DIC from four seasonal glider deployments in the MAB (W = winter, Sp = spring, Su = summer, and F = fall). Data shown are from the first cross-shelf transect of each deployment. Mixed layer depth (MLD) for each binned profile is plotted in white. Winter had no significant mixed layer. The nearshore region was defined as 1–40 km offshore, midshelf was 40–160 km offshore (40–120 km in spring), and the shelf break was >160 km offshore (>120 km offshore in spring).

4.1. Drivers of MAB Seasonality

Seasonal glider deployments recorded physical water column changes caused by intense MAB seasonality. Observations aligned with established MAB physical climatology (Castelao et al., 2010, 2008). Warming of surface waters in the spring and summer, combined with freshening of surface waters, increased the strength of stratification and trapped a Cold Pool water mass below the mixed layer. Cold Pool bottom water generally contains relatively fresh (<34 PSU) and cold (<10°C) water, with source water likely originating from the Labrador Sea (Z. Chen et al., 2018). Wind- and storm-driven seasonal overturn in the fall caused surface and Cold Pool bottom waters to mix, resulting in a cool, well-mixed water column that persisted through winter.

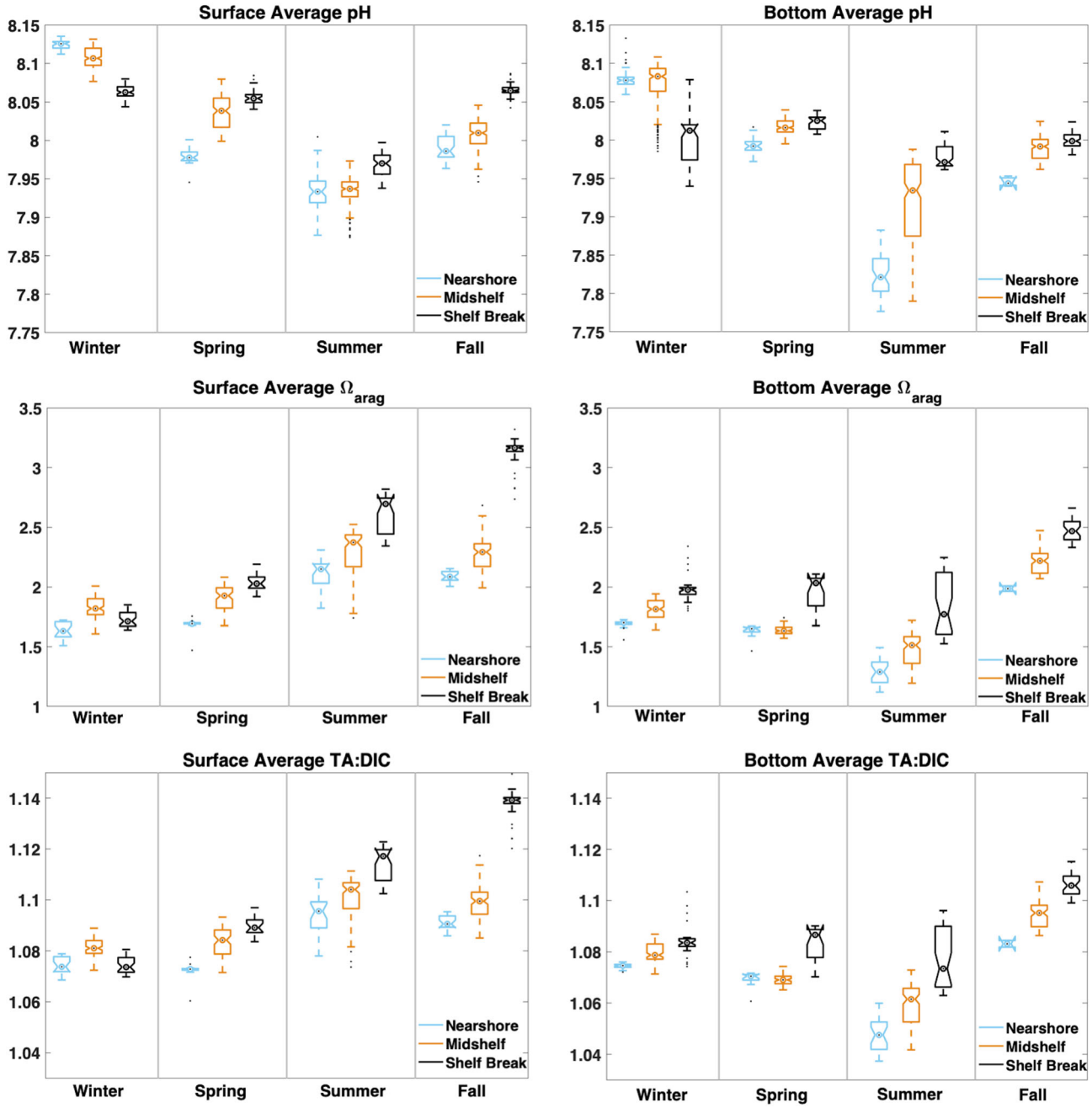

Figure 7. Comparisons of carbonate system parameters measured during and derived from seasonal glider deployments. Targets indicate median values, box limits indicate the 25th to 75th percentiles, and whiskers represent the full range of data. Data points beyond 1.5 times the interquartile range away from the top or bottom of the box were identified as outliers and are shown as black dots extending from the whiskers. Notches depict the 95% confidence interval around the median. If notches do not overlap, there is 95% confidence that the medians are different ($p < 0.05$).

The occurrence of low surface water Ω_{arag} and TA:DIC in winter and high Ω_{arag} and TA:DIC in summer surface waters supports the findings of Cai et al. (2020) who concluded that surface water Ω_{arag} and DIC are controlled additively by thermodynamic equilibrium and air-sea gas exchange in the MAB. Unlike Ω_{arag} and TA:DIC, shelf surface water pH during glider deployments exhibited a decoupling from the effect of gas exchange, with the highest pH recorded in winter and lowest pH values in summer. This indicated a more complicated system of seasonal surface pH drivers, including freshwater input (summer) and biological removal of CO_2 (winter), which acted on a time scale faster than gas equilibrium (Cai et al., 2020).

In areas and periods of dense chlorophyll biomass, primary producers remove CO_2 from the water, increasing DO and pH (Kemp et al., 1994). Fall and spring glider missions captured the highest seasonal integrated chlorophyll levels, due to high phytoplankton biomass. High fall integrated chlorophyll supports the findings of Y. Xu et al. (2011), who identified a bimodal cycle of biological production in the MAB, in which a dominant fall-winter phytoplankton bloom between the 20- and 60-m isobaths accounts for almost 60% of the region's annual chlorophyll production. This bloom forms when fall overturn injects nutrient-rich bottom water into the surface, promoting phytoplankton production. High productivity captured in the fall deployment led to high integrated DO and increased surface pH in the nearshore and midshelf. The second mode of MAB phytoplankton production described by Y. Xu et al. (2011) indicates a less dominant spring-summer bloom triggered by stratification, which allows phytoplankton to overcome light limitation caused by deep mixing during the winter. Spring and summer glider deployments captured the development of strong seasonal stratification, isolating a chlorophyll maximum just below the mixed layer predominantly in the midshelf region that was colocated with high pH (Figure 6).

High depth-integrated chlorophyll and DO in the fall and spring were followed by periods of lower integrated chlorophyll and DO in the winter and summer. In summer, this was likely influenced by Cold Pool bottom water, where respiration of surface-derived particulate carbon produces CO_2 and reduces DO. Once seasonal stratification is set up, the Cold Pool has little ventilation to seawater above the thermocline, and accumulation of respired CO_2 reduces pH, Ω_{arag}, and buffering capacity for CO_2 (Cai et al., 2011, 2017; Waldbusser & Salisbury, 2014; Wootton et al., 2008). Our summer mission captured the full extent of low bottom water pH, Ω_{arag}, and TA:DIC associated with stratification and the Cold Pool (Figures 6 and 7).

In summer nearshore surface and bottom waters, high-low-high cycles in pH, Ω_{arag}, and TA:DIC appeared in ~20-km increments (Figure 8). Cycles observed there align with the glider's average horizontal movement of 20 km day^{-1}, indicating potential diel variability in pH, Ω_{arag}, and TA:DIC. Daily swings in surface water pH were as large as 0.145 pH units, corresponding to swings in surface Ω_{arag} of 0.52 and TA:DIC of 0.033. These pH swings were about half the amplitude of those observed previously in nearby Mid-Atlantic estuaries, which can exhibit swings of up to 0.26 pH units day^{-1}, attributed to high productivity and shallow waters (Baumann & Smith, 2017). The pattern of daily variability was not always consistent (day vs. night), suggesting that these complex carbonate chemistry dynamics are likely driven by a combination of biological productivity, temperature swings, fluctuations in salinity, and mixing. For example, pH and Ω_{arag} in nearshore bottom water exhibited strong positive correlations with temperature and chlorophyll (Spearman's $r > 0.75$, $p < 0.001$) and strong negative correlations with salinity (Spearman's $r < -0.67$, $p < 0.001$). In nearshore surface water, these correlations were weaker and, in one case, the direction of the correlation flipped (Spearman's r between Ω_{arag} and chlorophyll $= -0.50$, $p < 0.001$). Therefore, trends in pH and Ω_{arag} cannot be explained by any one driver. Additional observations are needed in order to thoroughly analyze and establish the relative importance of these drivers to diel variability.

4.2. Year-Round Water Column Features

In every season, nearshore waters experienced the lowest surface salinities, highlighting the influence of freshwater inputs to the coastal system (Castelao et al., 2010). During the summer, freshening extended into the midshelf due to heavy rainfall and typical seasonal freshening due to peak seasonal runoff from the Hudson River (Castelao et al., 2010; Richaud et al., 2016). Freshwater inputs from rivers and storms introduce low TA water into the coastal system, decreasing CO_2 buffering capacity (Siedlecki et al., 2017; Waldbusser & Salisbury, 2014). Spring, summer, and fall exhibited their lowest respective pH, Ω_{arag}, and TA:DIC in nearshore waters compared to the midshelf and shelf break regions. Summer nearshore and midshelf surface waters had the lowest seasonal pH, pointing to freshwater input as a major driver of pH there. However, as discussed in section 4.1, summer nearshore and midshelf surface waters had the highest seasonal Ω_{arag} and TA:DIC, indicating that thermodynamic control was a stronger influence on Ω_{arag} and TA:DIC than salinity. These complex carbonate system dynamics indicate that freshwater influence is a complicated but important driver of the carbonate system on the shelf.

Throughout all seasonal deployments, a warm (>12°C), salty (>35 PSU) water mass persisted at the continental shelf break. This slope water mass signified that the glider traveled through a shelf-break front, formally called the MAB shelf-break jet, which is influenced by warm, saline Gulf Stream waters entrained into

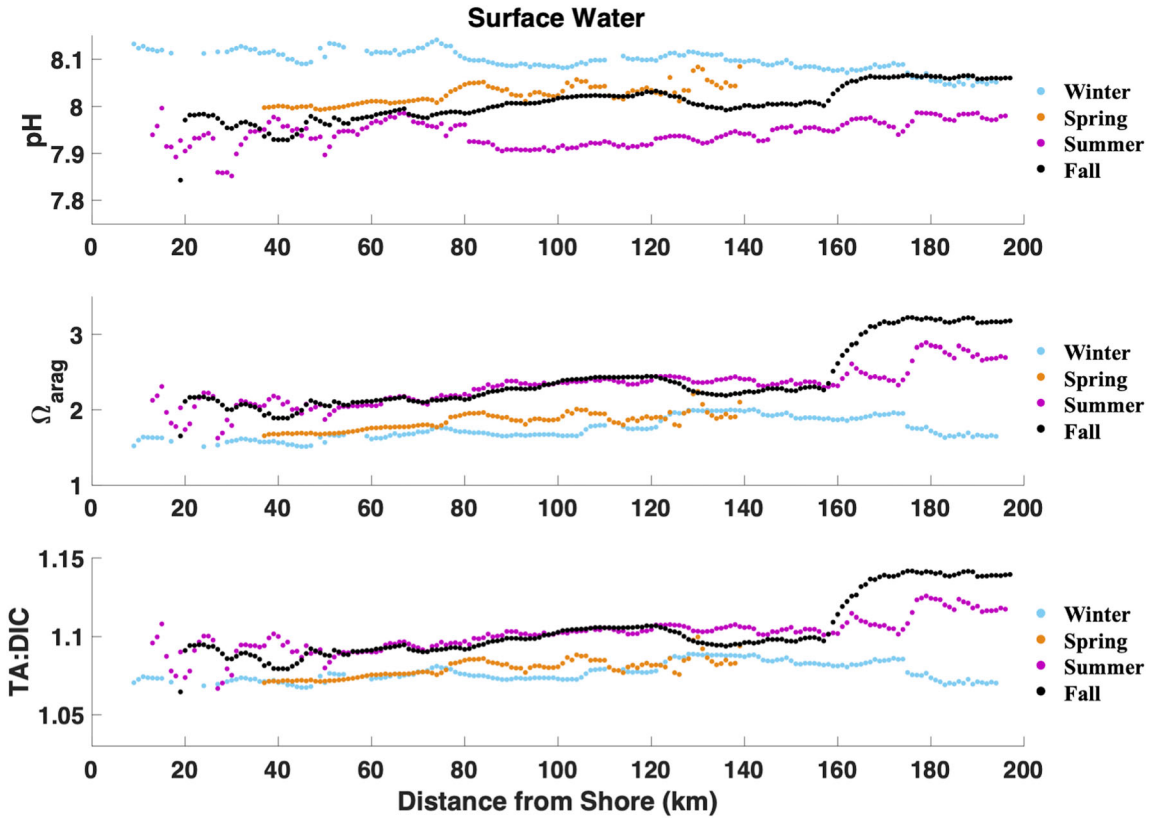

Figure 8. Seasonal differences in surface water pH (top), Ω_{arag} (middle), and TA:DIC (bottom) expressed as a function of distance from shore. Surface water is defined as above MLD in spring, summer, and fall, and as the top 5 m in winter. Data presented are from the entire deployment and are 1 m depth and 1 km distance binned.

the MAB by eddies (K. Chen & He, 2010; Fratantoni et al., 2001; Linder & Gawarkiewicz, 1998; Wanninkhof et al., 2015). The front was pushed progressively farther off-shelf with the onset and persistence of seasonal stratification and infiltrated back onto the shelf during fall overturn, following MAB shelf-break jet climatology described by Linder and Gawarkiewicz (1998). The deepest water sampled at the shelf break (>150 m) exhibited the lowest depth-averaged oxygen levels in each deployment, suggesting that this water mass is not well ventilated to the atmosphere, and ongoing respiration there depletes oxygen and adds CO_2. Despite ongoing respiration, shelf break jet deep water had high Ω_{arag} and TA:DIC, reflecting its Gulf Stream source and consistently high salinity levels. High TA:DIC indicated that this water mass had a high buffering capacity for CO_2 and therefore had high pH in spring, summer, and fall, regardless of high net respiration.

The intrusion of the highly buffered shelf break jet onto the shelf during fall overturn, along with the high fall phytoplankton biomass and a decrease in freshwater input, resulted in a well-mixed water column with high pH, Ω_{arag}, and TA:DIC. High pH persisted through winter, while thermodynamic interactions led to low winter Ω_{arag} and TA:DIC after the fall bloom. This suggests that seasonal intrusion of the shelf break jet could be an important mitigator of acidification on the MAB shelf during fall.

4.3. Potential Ecological Implications

It is important to consider natural seasonal, spatial, and depth variability when investigating MAB habitat suitability. Surface water pH, Ω_{arag}, and TA:DIC exhibited seasonal differences across the MAB shelf, with Ω_{arag} and TA:DIC diverging to a greater extent at the shelf break (Figure 8). Bottom water pH exhibited seasonal swings on the MAB shelf, but values converged at the continental shelf break, while bottom water Ω_{arag} and TA:DIC saw seasonal divergence at the shelf break (Figure 9). Seasonality in pH, Ω_{arag}, and TA:DIC across the shelf and shelf break demonstrated seasonal and spatial fluctuations in carbonate system drivers in the MAB.

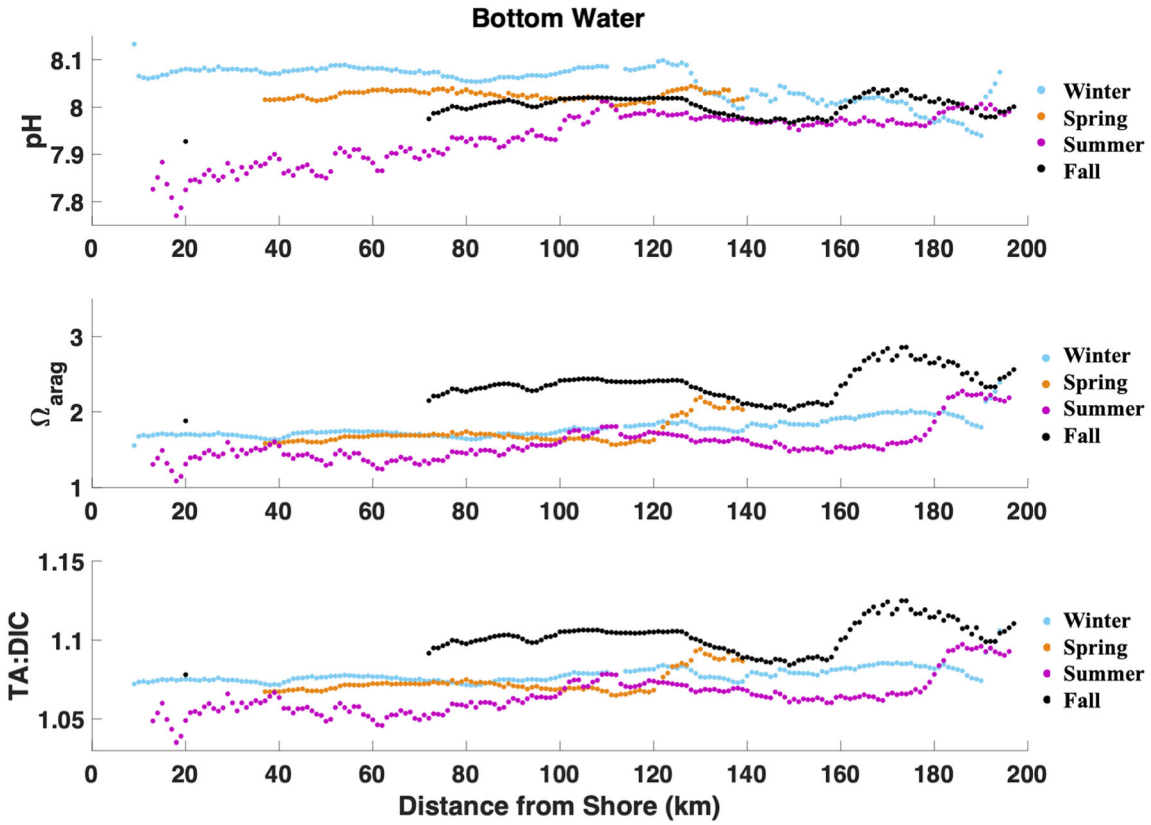

Figure 9. Seasonal differences in bottom water pH (top), Ω_{arag} (middle), and TA:DIC (bottom) expressed as a function of distance from shore. Bottom water is defined as below MLD in spring, summer, and fall, and as the bottom 5 m in winter. Data presented are from the entire deployment and are 1 m depth and 1 km distance binned.

Shelf water masses, specifically the MAB Cold Pool, have been linked to the distribution and recruitment of economically important fish species, including the calcifying shellfish Atlantic sea scallop (*Placopecten magellanicus*) and Atlantic surfclam (*Spisula solidissima*), which are vulnerable to acidification (Colvocoresses & Musick, 1984; Cooley et al., 2015; Steves et al., 2000; Sullivan et al., 2000; Weinberg, 2005). These organisms are able to survive and reproduce through observed seasonal swings in carbonate chemistry on the MAB shelf, but the extent to which survival and reproduction may be negatively impacted by current levels of pH and Ω_{arag} is unknown. Potential vulnerability of these organisms during late summer/early fall spawning events on the MAB shelf should be a consideration for future fishery management.

4.4. Limitations and Benefits

While the pH glider has undergone significant field testing for robustness, it is not exempt from limitations common to autonomous underwater vehicles (AUVs) and other sensors used in oceanographic field work. Gliders deployed in areas of high productivity are subject to biofouling over time, which can increase offsets between glider and discrete pH measurements (Saba, Wright-Fairbanks, et al., 2019). Increased offsets from deployment to recovery in winter, summer, and fall might indicate biofouling throughout deployment. Primary production associated with algal biofouling near the sensor intake would remove CO_2 from water in close vicinity to the glider, thereby increasing pH. Additionally, biofouling from barnacles or juvenile bivalves can occur on gliders. Saba, Wright-Fairbanks, et al. (2019) reported an instance of biofouling by a juvenile clam which settled onto the glider pH sensor intake valve. In that case, respiration would decrease pH around the sensor. Increases in offsets over time can also occur due to pH sensor drift. Sensor drift generally arises due to a lack of full conditioning to Br^- anion in seawater and is a common issue for autonomous pH monitoring platforms (Johnson et al., 2016).

Seasonal TA-salinity relationships derived from discrete samples perform generally well when compared to the CANYON-B algorithm and discrete sample TA values. Large offsets between discrete and regression-based TA corresponded to a break in the TA-salinity relationship at approximately 30–31 PSU (Figure S1). These offsets were particularly large in summer and fall, with discrete and calculated TA differing by up to 51.1 and 87.6 μmol kg^{-1} respectively (Table S5). Uncertainty in Ω_{arag} and TA:DIC due to TA uncertainty was as extreme as −0.08 and 0.0013 (fall; Table S4). However, the difference between CANYON-B-estimated TA and salinity-derived TA was quite small, averaging ~0.1%. Because of this, we are confident that seasonal TA-salinity regressions are applicable to full glider deployments.

While none of the seasonal deployment pH offsets described here exceeded manufacturer specifications for the sensor, changes in offsets over time underscore the importance of taking discrete samples at each glider deployment and recovery to ensure continued accuracy and data quality. These missions therefore require a vessel with water sampling capabilities, but the data provided during the otherwise automated 30- to 60-day missions far outweigh the cost to collect data of this resolution during major research cruises (Schofield et al., 2010). Furthermore, gliders have proven their effectiveness for high-quality observations in a range of coastal and open ocean environments, including locations that are not conducive to vessel operation or human presence (e.g., polar environments and hurricane seas) (Testor et al., 2019).

5. Significance

The work presented here highlights the distinct capability of an autonomous Slocum glider equipped with a deep-ISFET based pH sensor to make highly accurate, high-resolution observations of the marine carbonate system. The use of pH glider technology can be scaled up to address regional, national, and global OA observing needs. Using this glider sensor suite, we have observed seasonal patterns in the carbonate system directly associated with changes in other physical, biological, and chemical properties. While it is beyond the scope of this paper to quantify the relative importance of different carbonate system drivers, these data make clear that several drivers impact the strength of acidification. These include air-sea CO_2 exchange, seasonal stratification, biological activity, and freshwater input, as well as physical mixing of the MAB shelf break front. Importantly, data presented here describe the typical seasonal patterns of carbonate system dynamics in the MAB, but absolute values will change from year-to-year due to differences in regional climate, temperature, precipitation, wind patterns, and storm activity. Continued seasonal glider observation efforts, together with other carbonate monitoring platforms, will assist in developing a mean carbonate chemistry climatology for the MAB. This will help to inform the design of laboratory experiments investigating the response of commercially important species to acidification using realized carbonate system values and variability (Goldsmith et al., 2019; Saba, Goldsmith, et al., 2019). Furthermore, ongoing monitoring efforts can be used to identify areas or time periods prone to acidification due to interaction with other potential stressors, and the derivation of synergistic relationships between these variables. Continued simultaneous collection of chemical, physical, and biological metrics will allow the development of algorithms linking carbonate chemistry to other ocean properties. These quantitative relationships are necessary to develop broader predictive forecast models for the coastal ecosystem, which will ultimately aid in fisheries management planning and mitigation of short-term acidification events in the MAB.

Data Availability Statement

Data supporting the conclusions made in this paper can be obtained online (at http://slocum-data.marine.rutgers.edu/erddap/search/index.html?page=1&itemsPerPage=1000&searchFor=ru30).

Acknowledgments

We thank Rutgers University Center for Ocean Observing Leadership (RU COOL) glider technicians: David Aragon, Nicole Waite, Chip Haldeman, Laura Nazzaro, and John Kerfoot for their efforts in glider preparation, deployment logistics, fieldwork, mission piloting, and data management. We also thank Rutgers undergraduate alumni Brandon Grosso and Laura Wiltsee for their dedicated work with gliders in the field and lab. We acknowledge RU COOL faculty Oscar Schofield, Scott Glen, Josh Kohut, and RU COOL manager Michael Crowley for facility support. We appreciate Yui Takeshita (Monterey Bay Aquarium Research Institute) for his support on data interpretation. Finally, we thank our colleagues at SeaBird Scientific including Dave Murphy, Cristina Orrico, Vlad Simontov, and Dave Walter, along with Clara Hulburt and Christopher DeCollibus at Teledyne Webb Research for their technical expertise and support. This project was funded by National Science Foundation's Ocean Technology and Interdisciplinary Coordination program (National Science Foundation [NSF] OCE1634520 and OCE1634582). E. W-F. received support from the Mid-Atlantic Sea Grant/NOAA OAP Graduate Research Fellowship (NA18OAR4170087) and the Rutgers University School of Environmental and Biological Sciences Excellence Fellowship.

References

Baumann, H., & Smith, E. M. (2017). Quantifying metabolically driven pH and oxygen fluctuations in US nearshore habitats at diel to interannual time scales. *Estuaries and Coasts*, *41*(4), 1102–1117. https://doi.org/10.1007/s12237-017-0321-3

Bittig, H. C., Steinhoff, T., Claustre, H., Fiedler, B., Williams, N. L., Sauzède, R., et al. (2018). An alternative to static climatologies: Robust estimation of open ocean CO_2 variables and nutrient concentrations from T, S, and O_2 data using Bayesian neural networks. *Frontiers in Marine Science*, *5*. https://doi.org/10.3389/fmars.2018.00328

Bresnahan, P. J., Martz, T. R., Takeshita, Y., Johnson, K. S., & LaShomb, M. (2014). Best practices for autonomous measurement of seawater pH with the Honeywell Durafet. *Methods in Oceanography*, *9*, 44–60. https://doi.org/10.1016/j.mio.2014.08.003

Cai, W.-J., Hu, X., Huang, W.-J., Jiang, L.-Q., Wang, Y., Peng, T.-H., & Zhang, X. (2010). Alkalinity distribution in the western North Atlantic Ocean margins. *Journal of Geophysical Research*, *115*, C08014. https://doi.org/10.1029/2009JC005482

Cai, W.-J., Hu, X., Huang, W.-J., Murrell, M. C., Lehrter, J. C., Lohrenz, S. E., et al. (2011). Acidification of subsurface coastal waters enhanced by eutrophication. *Nature Geoscience*, *4*(11), 766–770. https://doi.org/10.1038/ngeo1297

Cai, W.-J., Huang, W. J., Luther, G. W. 3rd, Pierrot, D., Li, M., Testa, J., et al. (2017). Redox reactions and weak buffering capacity lead to acidification in the Chesapeake Bay. *Nature Communications*, *8*(1), 369. https://doi.org/10.1038/s41467-017-00417-7

Cai, W.-J., Xu, Y. Y., Feely, R. A., Wanninkhof, R., Jonsson, B., Alin, S. R., et al. (2020). Controls on surface water carbonate chemistry along North American ocean margins. *Nature Communications*, *11*(1), 2691. https://doi.org/10.1038/s41467-020-16530-z

Carvalho, F., Kohut, J., Oliver, M. J., & Schofield, O. (2017). Defining the ecologically relevant mixed-layer depth for Antarctica's coastal seas. *Geophysical Research Letters*, *44*, 338–345. https://doi.org/10.1002/2016GL071205

Castelao, R., Glenn, S., & Schofield, O. (2010). Temperature, salinity, and density variability in the central Middle Atlantic Bight. *Journal of Geophysical Research*, *115*, C10005. https://doi.org/10.1029/2009JC006082

Castelao, R., Glenn, S., Schofield, O., Chant, R., Wilkin, J., & Kohut, J. (2008). Seasonal evolution of hydrographic fields in the central middle Atlantic bight from glider observations. *Geophysical Research Letters*, *35*, L03617. https://doi.org/10.1029/2007GL032335

Chen, B., Cai, W.-J., & Chen, L. (2015). The marine carbonate system of the Arctic Ocean: Assessment of internal consistency and sampling considerations, summer 2010. *Marine Chemistry*, *176*, 174–188. https://doi.org/10.1016/j.marchem.2015.09.007

Chen, K., & He, R. (2010). Numerical investigation of the Middle Atlantic Bight shelfbreak frontal circulation using a high-resolution ocean hindcast model. *Journal of Physical Oceanography*, *40*(5), 949–964. https://doi.org/10.1175/2009jpo4262.1

Chen, Z., Curchitser, E., Chant, R., & Kang, D. (2018). Seasonal variability of the cold pool over the Mid-Atlantic Bight continental shelf. *Journal of Geophysical Research: Oceans*, *123*, 8203–8226. https://doi.org/10.1029/2018JC014148

Clayton, T. D., & Byrne, R. H. (1993). Spectrophotometric seawater pH measurements: Total hydrogen ion concentration scale calibration of m-cresol purple and at-sea results. *Deep-Sea Research*, *40*(10), 2115–2129.

Colvocoresses, J. A., & Musick, J. A. (1984). Species associations and community composition of Middle Atlantic Bight continental shelf demersal fishes. VIMS Articles, 625.

Cooley, S. R., Rheuban, J. E., Hart, D. R., Luu, V., Glover, D. M., Hare, J. A., & Doney, S. C. (2015). An integrated assessment model for helping the United States sea scallop (*Placopecten magellanicus*) fishery plan ahead for ocean acidification and warming. *PLoS ONE*, *10*(5), e0124145. https://doi.org/10.1371/journal.pone.0124145

DelValls, T. A., & Dickson, A. G. (1998). The pH of buffers based on 2-amino-2-hydroxymethyl-1,3-propanediol ('tris') in synthetic sea water. *Deep Sea Research*, *45*, 1541–1554.

Dickson, A. (1990). Standard potential of the reaction: AgCl(s) + 1/2H2(g) = Ag(s) + HCl (aq), and the standard acidity constant of the ion HSO4- in synthetic sea water from 273.15 to 318.15 K. *Journal of Chemical Thermodynamics*, *22*, 113–127.

Dickson, A., & Millero, F. J. (1987). A comparison of the equilibrium constants for the dissociation of carbonic acid in seawater media. *Deep-Sea Research*, *34*(10), 1733–1743.

Dlugokencky, E., & Tans, P. (2020). Trends in atmospheric carbon dioxide. NOAA Earth System Research Laboratory.

Doney, S. C., Fabry, V. J., Feely, R. A., & Kleypas, J. A. (2009). Ocean acidification: The other CO_2 problem. *Annual Review of Marine Science*, *1*, 169–192. https://doi.org/10.1146/annurev.marine.010908.163834

Egleston, E. S., Sabine, C. L., & Morel, F. M. M. (2010). Revelle revisited: Buffer factors that quantify the response of ocean chemistry to changes in DIC and alkalinity. *Global Biogeochemical Cycles*, *24*, GB1002. https://doi.org/10.1029/2008GB003407

Fratantoni, P. S., Pickart, R. S., Torres, D. J., & Scotti, A. (2001). Mean structure and dynamics of the shelfbreak jet in the Middle Atlantic Bight during fall and winter. *Journal of Physical Oceanography*, *31*, 2135–2156.

Friedrich, T., Timmermann, A., Abe-Ouchi, A., Bates, N. R., Chikamoto, M. O., Church, M. J., et al. (2012). Detecting regional anthropogenic trends in ocean acidification against natural variability. *Nature Climate Change*, *2*(3), 167–171. https://doi.org/10.1038/nclimate1372

Gattuso, J., Magnan, A., Bille, R., Cheung, W. W. L., Howes, E. L., Joos, F., et al. (2015). Contrasting futures for ocean and society from different anthropogenic CO_2 emissions scenarios. *Science Magazine*, *349*(6243). https://doi.org/10.1126/10.1126/science.aac4722

Gazeau, F., Quiblier, C., Jansen, J. M., Gattuso, J.-P., Middelburg, J. J., & Heip, C. H. R. (2007). Impact of elevated CO_2 on shellfish calcification. *Geophysical Research Letters*, *34*, L07603. https://doi.org/10.1029/2006GL028554

Gledhill, D., White, M., Salisbury, J., Thomas, H., Misna, I., Liebman, M., et al. (2015). Ocean and coastal acidification off New England and Nova Scotia. *Oceanography*, *25*(2), 182–197. https://doi.org/10.5670/oceanog.2015.41

Gobler, C. J., & Talmage, S. C. (2013). Short- and long-term consequences of larval stage exposure to constantly and ephemerally elevated carbon dioxide for marine bivalve populations. *Biogeosciences*, *10*(4), 2241–2253. https://doi.org/10.5194/bg-10-2241-2013

Gobler, C. J., & Talmage, S. C. (2014). Physiological response and resilience of early life-stage eastern oysters (*Crassostrea virginica*) to past, present and future ocean acidification. *Conservation Physiology*, *2*(1), cou004. https://doi.org/10.1093/conphys/cou004

Goldsmith, K. A., Lau, S., Poach, M. E., Sakowicz, G. P., Trice, T. M., Ono, C. R., et al. (2019). Scientific considerations for acidification monitoring in the U.S. Mid-Atlantic Region. *Estuarine, Coastal and Shelf Science*, *225*. https://doi.org/10.1016/j.ecss.2019.04.023

Gruber, N., Clement, D., Carter, B. R., Feely, R. A., van Heuven, S., Hoppema, M., et al. (2019). THe oceanic sink for anthropogenic CO_2 from 1994 to 2007. *Science*, *363*, 1193–1199.

Hare, J. A., Morrison, W. E., Nelson, M. W., Stachura, M. M., Teeters, E. J., Griffis, R. B., et al. (2016). A vulnerability assessment of fish and invertebrates to climate change on the northeast U. S. continental shelf. *PLoS ONE*, *11*(2), e0146756. https://doi.org/10.1371/journal.pone.0146756

Hettinger, A., Sanford, E., Hill, T. M., Russell, A. D., Sato, K. N. S., Hoey, J., et al. (2012). Persisten carry-over effects of planktonic exposure to ocean acidification in the Olympic oyster. *Eology*, *93*(12), 2758–2768.

Houghton, R. W., Shlitz, R., Beardsley, R. C., Butman, B., & Chamberlin, J. L. (1982). The Middle Atlantic Bight Cold Pool: Evolution of the temperature structure during summer 1979. *American Meteoroligcal Society*, *12*, 1019–1029.

Huang, W.-J., Wang, Y., & Cai, W.-J. (2012). Assessment of sample storage techniques for total alkalinity and dissolved inorganic carbon in seawater. *Limnology and Oceanography: Methods*, *10*(9), 711–717. https://doi.org/10.4319/lom.2012.10.711

Huret, M., Bourriau, P., Doray, M., Gohin, F., & Petitgas, P. (2018). Survey timing vs. ecosystem scheduling: Degree-days to underpin observed interannual variability in marine ecosystems. *Progress in Oceanography*, *166*, 30–40. https://doi.org/10.1016/j.pocean.2017.07.007

IOOS. (2019). Manual for real-time quality control of pH data observations: A guide to quality control and quality assurance for pH observations. https://doi.org/10.25923/111k-br08

IPCC. (2019). Summary for policymakers. IPCC special report on the ocean and cryosphere in a changing climate.

Johnson, K. S., Jannasch, H. W., Coletti, L. J., Elrod, V. A., Martz, T. R., Takeshita, Y., et al. (2016). Deep-Sea DuraFET: A pressure tolerant pH sensor designed for global sensor networks. *Analytical Chemistry*, *88*(6), 3249–3256. https://doi.org/10.1021/acs.analchem.5b04653

Johnson, K. S., Plant, J. N., & Maurer, T. L. (2017). Processing BGC-Argo ph data at the DAC level. https://doi.org/10.13155/57195
Kemp, P. F., Falkowski, P. G., Flagg, C. N., Phoel, W. C., Smith, S. L., Wallace, D. W. R., & Wirick, C. D. (1994). Modeling vertical oxygen and carbon flux during stratified spring and summer conditions on the continental shelf, Middle Atlantic Bight, eastern U. S. A. *Deep Sea Research*, *41*(2/3), 629–655.
Kohut, J., Haldeman, C., & Kerfoot, J. (2014). Monitoring dissolved oxygen in New Jersey coastal waters using autonomous gliders. Environmental Protection Agency Office of Research and Developmoent.
Levin, J., Wilkin, J., Fleming, N., & Zavala-Garay, J. (2018). Mean circulation of the Mid-Atlantic Bight from a climatological data assimilative model. *Ocean Modelling*, *128*, 1–14. https://doi.org/10.1016/j.ocemod.2018.05.003
Lewis, E., & Wallace, D. W. R. (1998). Program developed for CO_2 system calculations.
Linder, C. A., & Gawarkiewicz, G. (1998). A climatology of the shelfbreak front in the Middle Atlantic Bight. *Journal of Geophysical Research*, *103*(C9), 18,405–18,423. https://doi.org/10.1029/98JC01438
Liu, X., Patsavas, M. C., & Byrne, R. H. (2011). Purification and characterization of meta-cresol purple for spectrophotometric seawater pH measurements. *Environmental Science & Technology*, *45*(11), 4862–4868. https://doi.org/10.1021/es200665d
Lorbacher, K., Dommenget, D., Niiler, P. P., & Köhl, A. (2006). Ocean mixed layer depth: A subsurface proxy of ocean-atmosphere variability. *Journal of Geophysical Research*, *111*, C07010. https://doi.org/10.1029/2003JC002157
Martz, T. R., McLaughlin, K., & Weisberg, S. (2015). Best Practices for autonomous measurement of seawater pH with the Honeywell Durafet pH sensor. California Current Acidification Network (C-CAN).
Mehrbach, C., Culberson, C. H., Hawley, J. E., & Pytkowicz, R. M. (1973). Measurement of the apparent dissociation constants of carbonic acid in seawater at atmospheric pressure. *Limnology and Oceanography*, *18*(6), 897–907.
Melzner, F., Mark, F. C., Seibel, B. A., & Tomanek, L. (2019). Ocean acidification and coastal marine invertebrates: Tracking CO_2 effects from seawater to the cell. *Annual Review of Marine Science*, *12*, 12.11–12.25. https://doi.org/10.1146/annurev-marine-010419-010658
Miller, A. W., Reynolds, A. C., Sobrino, C., & Riedel, G. F. (2009). Shellfish face uncertain future in high CO_2 world: Influence of acidification on oyster larvae calcification and growth in estuaries. *PLoS ONE*, *4*(5), e5661. https://doi.org/10.1371/journal.pone.0005661
Millero, F. J. (1986). The pH of estuarine waters. *Limnology and Oceanography*, *31*(4), 839–847.
Musial, W., Elliott, D., Fields, J., Parker, Z., Scott, G., & Draxl, C. (2013). Assessment of offshore wind energy leasing areas for the BOEM New Jersey wind energy area. National Renewable Energy Laboratory Technical Reports.
NEFSC. (2020). State of the ecosystem 2020: Mid-Atlantic. NOAA Fisheries Reports.
NRC (2010). *Ocean acidification: A national strategy to meet the challenges of a changing ocean*. New York: The National, Academies Press. https://doi.org/10.17226/12904
Orr, J. C., Fabry, V. J., Aumont, O., Bopp, L., Doney, S. C., Feely, R. A., et al. (2005). Anthropogenic ocean acidification over the twenty-first century and its impact on calcifying organisms. *Nature*, *437*(7059), 681–686. https://doi.org/10.1038/nature04095
Pan, T. C., Applebaum, S. L., & Manahan, D. T. (2015). Experimental ocean acidification alters the allocation of metabolic energy. *Proceedings of the National Academy of Sciences of the United States of America*, *112*(15), 4696–4701. https://doi.org/10.1073/pnas.1416967112
Perez, F. F., & Fraga, F. (1987). Association constant of fluoride and hydrogen ions in seawater. *Marine Chemistry*, *21*(2), 161–168. https://doi.org/10.1016/0304-4203(87)90036-3
Pimenta, A. R., & Grear, J. S. (2018). Guidelines for measuring changes in seawater pH and associated carbonate chemistry in coastal environments of the eastern United States. United States Environmental Protection Agency.
Richaud, B., Kwon, Y.-O., Joyce, T. M., Fratantoni, P. S., & Lentz, S. J. (2016). Surface and bottom temperature and salinity climatology along the continental shelf off the Canadian and U.S. East Coasts. *Continental Shelf Research*, *124*, 165–181. https://doi.org/10.1016/j.csr.2016.06.005
Rudnick, D. L. (2016). Ocean research enabled by underwater gliders. *Annual Review of Marine Science*, *8*, 519–541. https://doi.org/10.1146/annurev-marine-122414-033913
Runcie, J. W., Krause, C., Torres Gabarda, S. A., & Byrne, M. (2018). Technical note: Continuous fluorescence-based monitoring of seawater pH in situ. *Biogeosciences*, *15*(13), 4291–4299. https://doi.org/10.5194/bg-15-4291-2018
Saba, G. K., Goldsmith, K. A., Cooley, S. R., Grosse, D., Meseck, S. L., Miller, A. W., et al. (2019). Recommended priorities for research on ecological impacts of ocean and coastal acidification in the U.S. Mid-Atlantic. *Estuarine, Coastal and Shelf Science*, *225*, 106188. https://doi.org/10.1016/j.ecss.2019.04.022
Saba, G. K., Wright-Fairbanks, E., Chen, B., Cai, W.-J., Barnard, A. H., Jones, C. P., et al. (2019). The development and validation of a profiling glider deep ISFET-based pH sensor for high resolution observations of coastal and ocean acidification. *Frontiers in Marine Science*, *6*. https://doi.org/10.3389/fmars.2019.00664
Salisbury, J., Vandemark, D., Jönsson, B., Balch, W., Chakraborty, S., Lohrenz, S., et al. (2015). How can present and future satellite missions support scientific studies that address ocean acidification? *Oceanography*, *25*(2), 108–121. https://doi.org/10.5670/oceanog.2015.35
Schofield, O., Kohut, J., Aragon, D., Creed, L., Graver, J., Haldeman, C., et al. (2007). Slocum gliders: Robust and ready. *Journal of Field Robotics*, *24*(6), 473–485. https://doi.org/10.1002/rob.20200
Schofield, O., Kohut, J., Glenn, S., Morell, J. M., Capella, J., Corredor, J., et al. (2010). A regional Slocum glider network in the Mid-Atlantic Bight leverages broad community engagement. *Marine Technology Society Journal*, *44*(6).
Sharp, J. D., Pierrot, D., Humphreys, M. P., Epitalon, J.-M., Orr, J. C., Lewis, E., & Wallace, D. W. R. (2020). CO_2-System-Extd, v3.0, MATLAB (MathWorks).
Siedlecki, S. A., Pilcher, D. J., Hermann, A. J., Coyle, K., & Mathis, J. (2017). The importance of freshwater to spatial variability of aragonite saturation state in the Gulf of Alaska. *Journal of Geophysical Research: Oceans*, *122*, 8482–8502. https://doi.org/10.1002/2017JC012791
Steves, B. P., Cowen, R. K., & Malchoff, M. H. (2000). Settlement and nursery habitats for demersal fishes on the continental shelf of the New York Bight. *Fishery Bulletin*, *98*(1), 167–188.
Sullivan, M. C., Cowen, R. K., Able, K. W., & Fahay, M. P. (2000). Spatial scaling of recruitment in four continental shelf fishes. *Marine Ecology Progress Series*, *207*, 141–154.
Sutton, A. J., Sabine, C. L., Feely, R. A., Cai, W.-J., Cronin, M. F., McPhaden, M. J., et al. (2016). Using present-day observations to detect when anthropogenic change forces surface ocean carbonate chemistry outside preindustrial bounds. *Biogeosciences*, *13*(17), 5065–5083. https://doi.org/10.5194/bg-13-5065-2016
Talmage, S. C., & Gobler, C. J. (2009). The effects of elevated carbon dioxide concentrations on the metamorphosis, size, and survival of larval hard clams (*Mercenaria mercenaria*), bay scallops (*Argopecten irradians*), and Eastern oysters (*Crassostrea virginica*). *Limnology and Oceanography*, *54*(6), 2072–2080.

Talmage, S. C., & Gobler, C. J. (2010). Effects of past, present, and future ocean carbon dioxide concentrations on the growth and survival of larval shellfish. *Proceedings of the National Academy of Sciences of the United States of America*, *107*(40), 17,246–17,251. https://doi.org/10.1073/pnas.0913804107

Testor, P., de Young, B., Rudnick, D. L., Glenn, S., Hayes, D., Lee, C. M., et al. (2019). OceanGliders: A component of the integrated GOOS. *Frontiers in Marine Science*, *6*. https://doi.org/10.3389/fmars.2019.00422

Uppstrom, L. (1974). The boron/chlorinity ratio of deep-sea water from the Pacific Ocean. *Deep-Sea Research*, *21*(2).

van Heuven, S., Pierrot, D., Rae, J. W. B., Lewis, E., & Wallace, D. W. R. (2011). MATLAB program developed for CO_2 system calculations. ORNL/CDIAC-105b. Carbon Dioxide Information Analysis Center, Oak Ridge National Laboratory, U.S. Department of Energy, Oak Ridge, Tennessee. https://doi.org/10.3334/CDIAC/otg.CO2SYS_MATLAB_v1.1

Waldbusser, G. G., Hales, B., Langdon, C. J., Haley, B. A., Schrader, P., Brunner, E. L., et al. (2014). Saturation-state sensitivity of marine bivalve larvae to ocean acidification. *Nature Climate Change*, *5*(3), 273–280. https://doi.org/10.1038/nclimate2479

Waldbusser, G. G., & Salisbury, J. E. (2014). Ocean acidification in the coastal zone from an organism's perspective: Multiple system parameters, frequency domains, and habitats. *Annual Review of Marine Science*, *6*, 221–247. https://doi.org/10.1146/annurev-marine-121211-172238

Wang, H., Hu, X., Cai, W.-J., & Sterba-Boatwright, B. (2017). Decadal fCO_2 trends in global ocean margins and adjacent boundary current-influenced areas. *Geophysical Research Letters*, *44*, 8962–8970. https://doi.org/10.1002/2017GL074724

Wang, Z. A., Wanninkhof, R., Cai, W.-J., Byrne, R. H., Hu, X., Peng, T.-H., & Huang, W.-J. (2013). The marine inorganic carbon system along the Gulf of Mexico and Atlantic coasts of the United States: Insights from a transregional coastal carbon study. *Limnology and Oceanography*, *58*(1), 325–342. https://doi.org/10.4319/lo.2013.58.1.0325

Wanninkhof, R., Barbero, L., Byrne, R., Cai, W.-J., Huang, W.-J., Zhang, J.-Z., et al. (2015). Ocean acidification along the Gulf Coast and East Coast of the USA. *Continental Shelf Research*, *98*, 54–71. https://doi.org/10.1016/j.csr.2015.02.008

Weinberg, J. R. (2005). Bathymetric shift in the distribution of Atlantic surfclams: Response to warmer ocean temperature. *ICES Journal of Marine Science*, *62*(7), 1444–1453. https://doi.org/10.1016/j.icesjms.2005.04.020

Wootton, J. T., Pfister, C. A., & Forester, J. D. (2008). Dynamic patterns and ecological impacts of declining ocean pH in a high-resolution multi-year dataset. *Proceedings of the National Academy of Sciences of the United States of America*, *105*(48), 18,848–18,853. https://doi.org/10.1073/pnas.0810079105

Xu, Y., Chant, R., Gong, D., Castelao, R., Glenn, S., & Schofield, O. (2011). Seasonal variability of chlorophyll a in the Mid-Atlantic Bight. *Continental Shelf Research*, *31*(16), 1640–1650. https://doi.org/10.1016/j.csr.2011.05.019

Xu, Y.-Y., Cai, W.-J., Gao, Y., Wanninkhof, R., Salisbury, J., Chen, B., et al. (2017). Short-term variability of aragonite saturation state in the central Mid-Atlantic Bight. *Journal of Geophysical Research: Oceans*, *122*, 4274–4290. https://doi.org/10.1002/2017JC012901

Xu, Y. Y., Cai, W. J., Wanninkhof, R., Salisbury, J., Reimer, J., & Chen, B. (2020). Long-term changes of carbonate chemistry variables along the north American East Coast. *Journal of Geophysical Research: Oceans*, *125*(7), e2019JC015982. https://doi.org/10.1029/2019JC015982

Zeebe, R. E. (2012). History of seawater carbonate chemistry, atmospheric CO_2, and ocean acidification. *Annual Review of Earth and Planetary Sciences*, *40*(1), 141–165. https://doi.org/10.1146/annurev-earth-042711-105521